Applied Computational Electromagnetics Society

March 2005

APPLIED COMPUTATIONAL ELECTROMAGNETICS SOCIETY (ACES)

NEWSLETTER

Vol. 20 No. 1   March 2005

TABLE OF CONTENTS

PERMANENT STANDING COMMITTEES OF ACES, INC.

COMMITTEE	CHAIRMAN	ADDRESS
NOMINATION	Rene Allard	Penn State University PO Box 30 State College, PA 16804-0030 rja5@psu.edu
ELECTIONS	Rene Allard	Penn State University PO Box 30 State College, PA 16804-0030 rja5@psu.edu
FINANCE	Andrew Peterson	Georgia Institute of Technology School of ECE Atlanta, GA 30332-0250 peterson@ece.gatech.edu
PUBLICATIONS	Atef Elsherbeni	EE Department, Anderson Hall University of Mississippi University, MS 38677 atef@olemiss.edu
CONFERENCE	Osama Mohammed	Florida International University ECE Department Miami, FL 33174 mohammed@fiu.edu
AWARDS	Ray Perez	Martin Marietta Astronautics MS 58700, PO Box 179 Denver, CO 80201 ray.j.perez@lmco.com

MEMBERSHIP ACTIVITY COMMITTEES OF ACES, INC.

COMMITTEE	ADDRESS	CHAIRMAN
SOFTWARE VALIDATION	Bruce Archambeault	IBM 3039 Cornwallis Road, PO Box 12195 Dept. 18DA B306 Research Triangle Park, NC 27709
HISTORICAL	Robert Bevensee	BOMA Enterprises PO Box 812 Alamo, CA 94507-0812 rmbevensee@cs.com
CONSTITUTION and BYLAWS	Leo Kempel	2120 Engineering Building Michigan State University East Lansing, MI 48824 kempel@egr.msu.edu
MEMBERSHIP and COMMUNICATIONS	Vicente Rodriguez	ETS-LINDGREN L.P. 1301 Arrow Point Drive Cedar Park, TX 78613 rodriguez@ieee.org
INDUSTRY RELATIONS	Andy Drodz	ANDRO Consulting Services PO Box 543 Rome, NY 13442-0543 andro1@aol.com

4

NEWSLETTER ARTICLES AND VOLUNTEERS WELCOME

The ACES Newsletter is always looking for articles, letters and short communications of interest to ACES members. All individuals are encouraged to write, suggest or solicit articles either on a one-time or continuing basis. Please contact a Newsletter Editor.

AUTHORSHIP AND BERNE COPYRIGHT CONVENTION

The opinions, statements and facts contained in this Newsletter are solely the opinions of the authors and/or sources identified with each article. Articles with no author can be attributed to the editors or to the committee head in the case of committee reports. The United States recently became part of the Berne Copyright Convention. Under the Berne Convention, the copyright for an article in this newsletter is legally held by the author(s) of the article since no explicit copyright notice appears in the newsletter.

Current Vector Alignment and Lowered Resonance in Small Planar HF Wire Antenna Designs

W. Perry Wheless, Jr.
Department of Electrical and Computer Engineering
The University of Alabama
Tuscaloosa, AL 35487
Email: wwheless@coe.eng.ua.edu

Abstract—**Current vector alignment is a significant guide to whether a proposed small HF antenna design will be effective in lowering resonant frequency as a function of total wire length. The effect is illustrated here through three case studies of planar designs for the 160-meter amateur radio band (1.8 - 2.0 MHz).**

I. INTRODUCTION

There is considerable interest in electrically small antennas. The discussion here is generally applicable, but is presented in the context of three small antenna candidates for the 160-meter amateur radio band so that quantitative illustrations are possible. A major conclusion of this study is that the minimum size of a resonant wire antenna remains an open consideration, despite pronouncements to the contrary. For example, the Hilbert curve fractal dipole (configuration sketched in Figure 1 [1]) is said by some to exhibit the lowest resonant frequency of any antenna of the same size.

For a resonant frequency at 1.9 MHz, the Hilbert curve fractal dipole would require a wire length of approximately 168.6 m and dimensions approximately 9.84 m × 9.84 m (based on a resonant frequency of 267 MHz for a wire length of 1.2 m and area 7 cm × 7 cm). However, a look at current vector alignment for this wire antenna geometry, shown in Figure 2, is immediately suggestive. The close proximity of many oppositely directed current vector segments indicates that this antenna actually should be expected to be relatively ineffective in lowering resonant frequency as a function of total wire length. It is easy to produce numerous examples that substantiate that conclusion, and lead to the premise of this paper that the wire antenna configuration that truly has the lowest resonant frequency for a given size (occupied planar area) remains open for discovery.
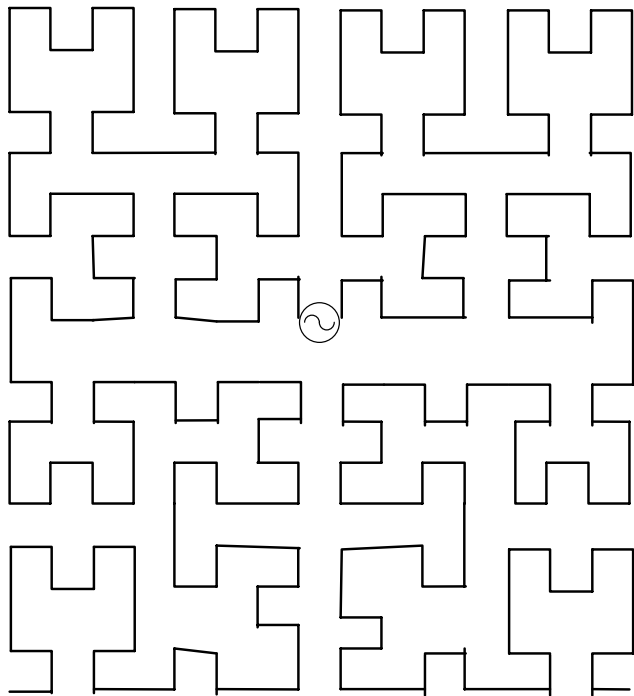

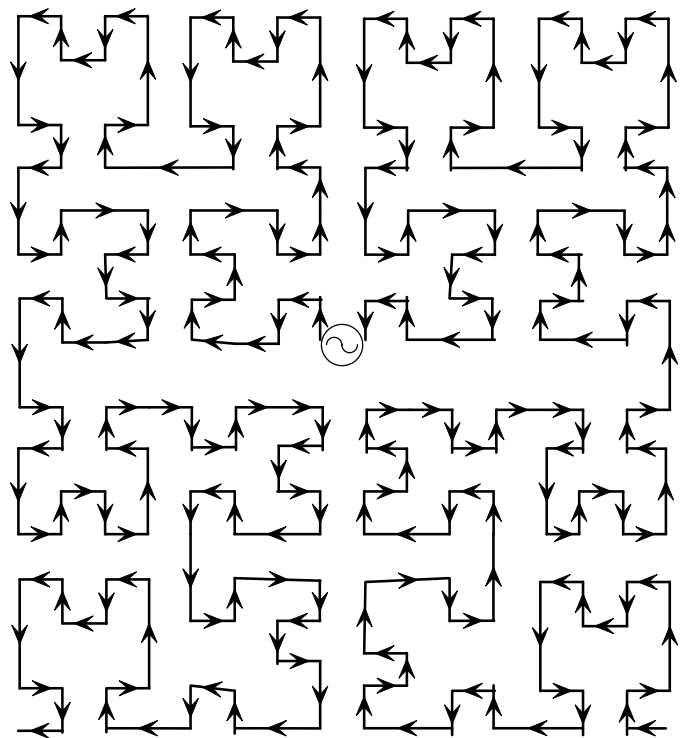Fig. 1. Hilbert Curve Fractal Dipole.

Fig. 2. Current vector alignment on Hilbert fractal dipole.

II. Current Vector Alignment

Generally speaking, when current vectors in close proximity oppose, the result is reduced radiation moment (i.e., more transmission line effect) which decreases the effective length of the antenna wire. On the other hand, when current vectors align both the radiation moment and the effective length of the antenna wire are increased. The condition to be emulated is clearly shown by the journeyman half-wave dipole:
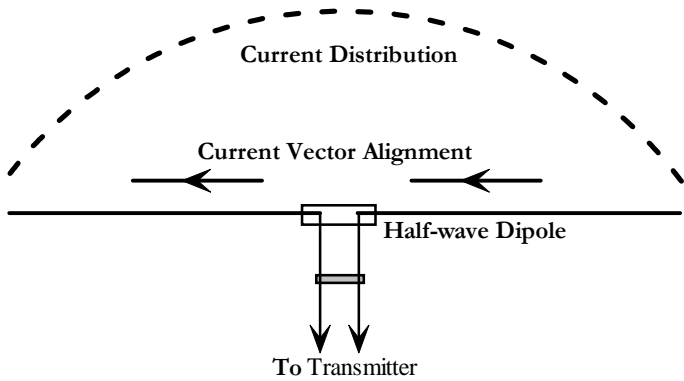
Fig. 3. Half-wave dipole current alignment.

III. Antenna 1

The first example of a configuration that will produce a lower resonant frequency within the constraint of a 7 cm × 7 cm size is offered in Figure 4.
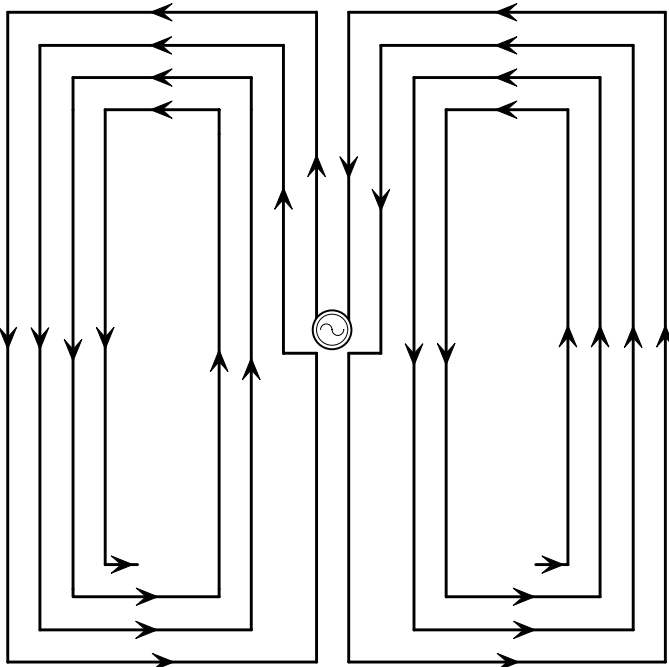
Fig. 4. Example 1 wire antenna configuration.

Here, current vector alignment indicates this antenna configuration whould be more effective in lowering resonant frequency as a function of total wire length. For a total wire length of 1.2 m and size 7 cm × 7 cm, the resonant frequency for this antenna is approximately 155 MHz, significantly lower than the 267 MHz resonance of the Hilbert fractal dipole. Directly scaling to 1.9 MHz, the total wire length becomes 98.7 m and the overall size is approximately 19.1 feet × 19.1 feet.

To analyze the attractiveness of this design as a 160-meter small antenna candidate, numerical modeling with EZNEC version 4.0 [2] was applied. For all EZNEC results reported here, real/high accuracy ground was selected with $\sigma = 3$ mS/m and $\epsilon_r = 12$, typical of west central Alabama soil conditions. Also, "copper" wire loss was selected, so the results here include conductor loss. In all cases, these planar antennas are vertically oriented (in the $y - z$ plane at $x = 0$), with +y corresponding to the compass direction North, and +x corresponding to the compass direction East. Therefore, in contemplating these example antennas in actual 160 m operation in the real world, azimuth angle $\varphi = 0°$ is toward the East, $\varphi = 90°$ is toward the North, and so forth.

Resonance with a very thin wire of 0.1 mm diameter has a (numerically) predicted feed-point impedance of $136 + j2 \ \Omega$, which is quite encouraging. Unfortunately, achieving resonance and a favorable feed-point impedance does not necessarily mean the antenna is an effective radiator. Figures 5a and 5b show the elevation patterns for azimuth $\varphi = 0°$ (East-West, broadside to the antenna plane) and $\varphi = 90°$ (North-South, in the plane of the antenna) with the bottom of the antenna only 1m above real ground, and gain of only about -21 dBi is clearly disappointing. A natural immediate question is whether the close proximity to ground is the cuprit, but raising the antenna bottom to 80m above ground only improves the gain by about 1 dB as shown in Figure 5c. Figure 5c does show, however, that the radiation pattern is significantly modified by raising the antenna up high in the air.

Most radio amateurs aspiring to operate on the 160-meter band from a space-restricted residential lot have at least enough room to accommodate a half-wave 75-m dipole. A full $\frac{\lambda}{2}$ dipole in free space has a gain of 2.15 dBi, and gain performance is generally expected to be a comparable value for an proposed alternative antenna system to be considered as a viable candidate. Since operating a 75m dipole as a half-sized dipole at 160m would give a gain penalty only in the -20 dBi range, the majority would probably opt for having good performance at 75m and -20 dBi gain at 160m from a single antenna, versus erecting both the planar 160m small Antenna 1 and a 75m dipole to cover the two bands.

However, several positive results have come from studying this design: (1) it shows one definitely can do better than the Hilbert fractal dipole with a given size limitation, (2) the resonant feed-point impedance is quite robust, (3) the size of this small 160m planar wire antenna is less than 20 feet on a side, and (4) adding current vector alignment as a consideration to our design toolkit boosts optimism for better future designs.
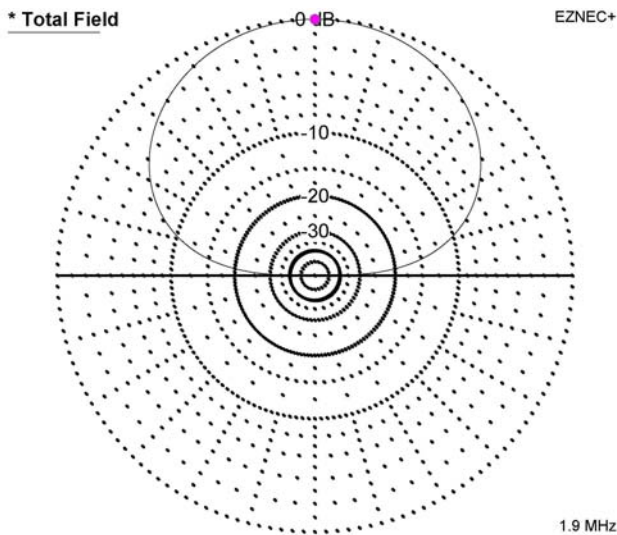
Example 1 small 160m antenna.

Elevation Plot		Cursor Elev	90.0 deg.
Azimuth Angle	0.0 deg.	Gain	-21.09 dBi
Outer Ring	-21.09 dBi		0.0 dBmax

Slice Max Gain	-21.09 dBi @ Elev Angle = 90.0 deg.
Beamwidth	96.6 deg.; -3dB @ 41.7, 138.3 deg.
Sidelobe Gain	< -100 dB
Front/Sidelobe	> 100 dB

Fig. 5a. Example 1 $\varphi = 0°$ elevation plot.

Example 1 small 160m antenna.

Elevation Plot		Cursor Elev	90.0 deg.
Azimuth Angle	90.0 deg.	Gain	-21.09 dBi
Outer Ring	-21.09 dBi		0.0 dBmax

Slice Max Gain	-21.09 dBi @ Elev Angle = 90.0 deg.
Beamwidth	138.4 deg.; -3dB @ 20.8, 159.2 deg.
Sidelobe Gain	< -100 dB
Front/Sidelobe	> 100 dB

Fig. 5b. Example 1 $\varphi = 90°$ elevation plot.
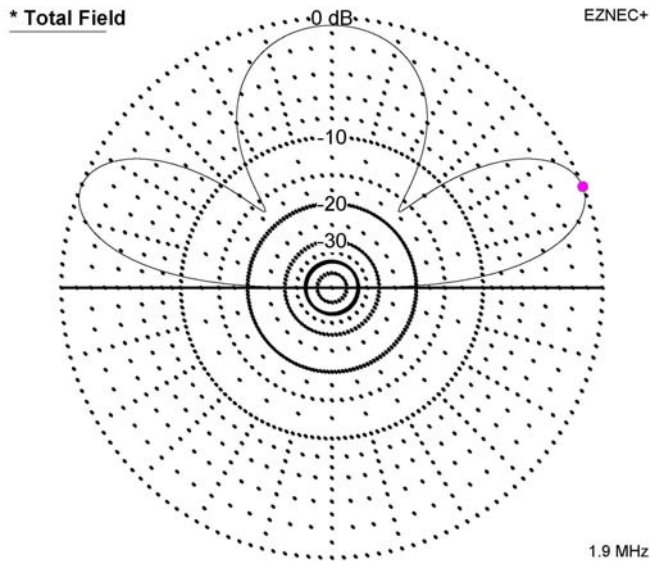
Example 1 small 160m antenna.

Elevation Plot		Cursor Elev	22.0 deg.
Azimuth Angle	0.0 deg.	Gain	-20.3 dBi
Outer Ring	-20.3 dBi		0.0 dBmax

Slice Max Gain	-20.3 dBi @ Elev Angle = 22.0 deg.
Beamwidth	23.8 deg.; -3dB @ 10.8, 34.6 deg.
Sidelobe Gain	-20.3 dBi @ Elev Angle = 158.0 deg.
Front/Sidelobe	0.0 dB

Fig. 5c. Example 1 $\varphi = 0°$ elevation plot, 80m height

IV. ANTENNA 2

The next candidate small 160m antenna to be presented has the geometry shown in Figure 6. A VHF implementation of this geometry with 0.54m of wire length exhibitied a resonant frequency about 245 MHz, implying that a version with 1.2m of wire would resonate at approximately 122 MHz, even lower than that of the Antenna 1 antenna above.

The total wire to make a 160m version of this antenna is approximately 73.2 meters, with overall size 30.2 feet × 30.2 feet. Using 2 mm antenna wire in the EZNEC modeling, now the feed-point impedance at resonance is about $7 + j24\ \Omega$. While this is an impedance that remains reasonably amenable to getting rf power into the antenna, it is obviously less than would be desired and much lower than that obtained from the Antenna 1 geometry.

Examining the currect vector alignment in Figure 6, some areas of field cancellation are apparent. On the other hand, there is less "folding" of wires in comparison to the Antenna 1 antenna and therefore the prospect for better radiation performance.

The three radiation patterns corresponding to those of Figure 5a-c for the Antenna 1 antenna are given below for the Antenna 2 configuration in Figure 7a-c. The patterns confirm that Antenna 2 is a superior radiator in comparison

to Antenna 1, at the expense of a somewhat more challenging feed-point impedance.
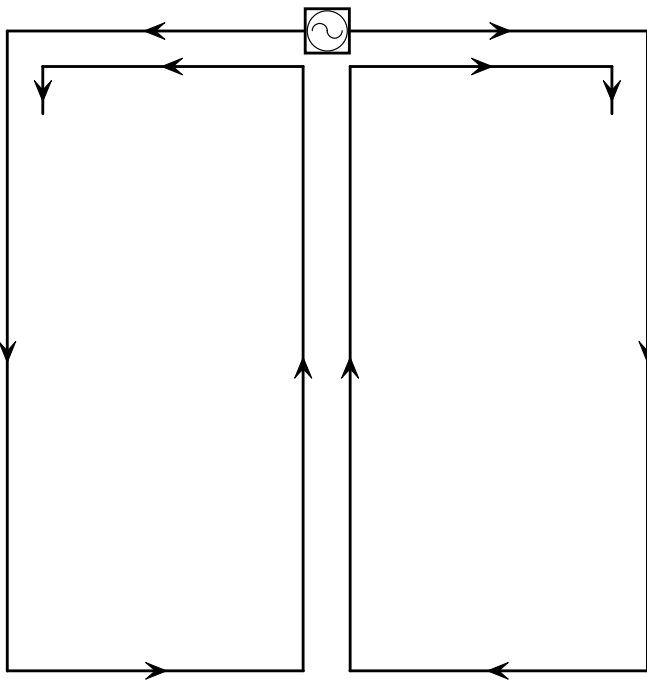
Fig. 6. Example 2 configuration.

Example 2 160m small antenna

Elevation Plot		Cursor Elev	90.0 deg.
Azimuth Angle	90.0 deg.	Gain	-4.36 dBi
Outer Ring	-4.36 dBi		0.0 dBmax

Slice Max Gain	-4.36 dBi @ Elev Angle = 90.0 deg.
Beamwidth	138.6 deg.; -3dB @ 20.7, 159.3 deg.
Sidelobe Gain	< -100 dBi
Front/Sidelobe	> 100 dB
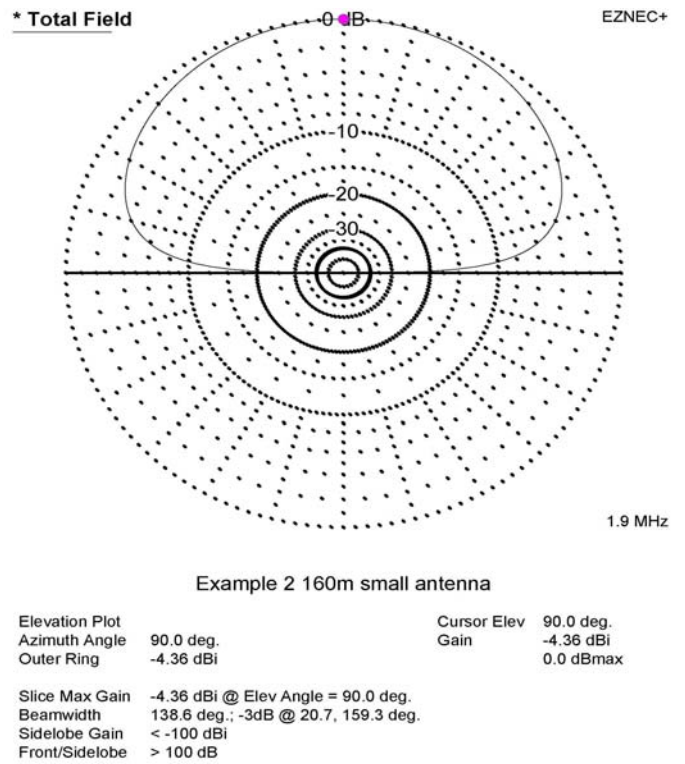
Fig. 7b. Example 2 $\varphi = 90°$ elevation plot.

Example 2 160m small antenna

Elevation Plot		Cursor Elev	90.0 deg.
Azimuth Angle	0.0 deg.	Gain	-4.36 dBi
Outer Ring	-4.36 dBi		0.0 dBmax

Slice Max Gain	-4.36 dBi @ Elev Angle = 90.0 deg.
Beamwidth	98.2 deg.; -3dB @ 40.9, 139.1 deg.
Sidelobe Gain	< -100 dBi
Front/Sidelobe	> 100 dB
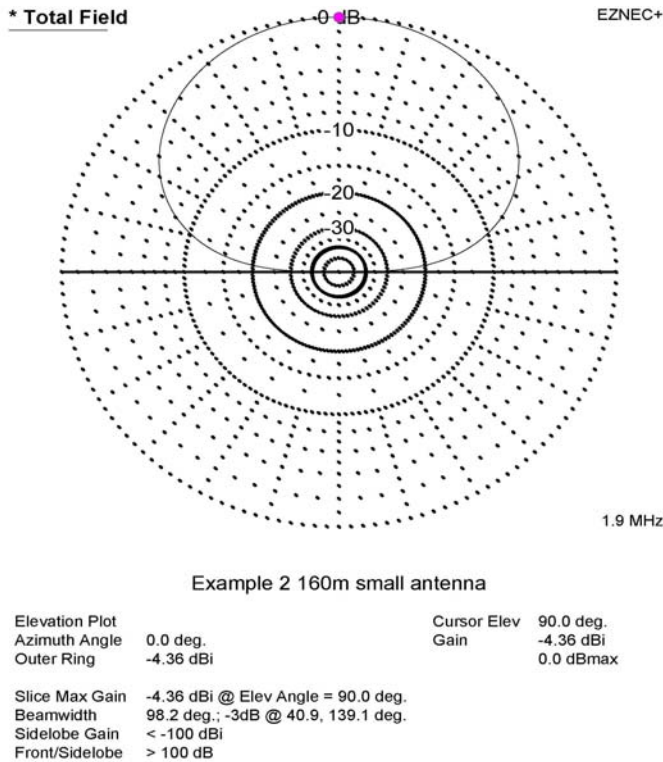
Fig. 7a. Example 2 $\varphi = 0°$ elevation plot.

Example 2 160m small antenna

Elevation Plot		Cursor Elev	90.0 deg.
Azimuth Angle	0.0 deg.	Gain	-1.63 dBi
Outer Ring	-1.63 dBi		0.0 dBmax

Slice Max Gain	-1.63 dBi @ Elev Angle = 90.0 deg.
Beamwidth	54.8 deg.; -3dB @ 62.6, 117.4 deg.
Sidelobe Gain	-3.19 dBi @ Elev Angle = 159.0 deg.
Front/Sidelobe	1.56 dB
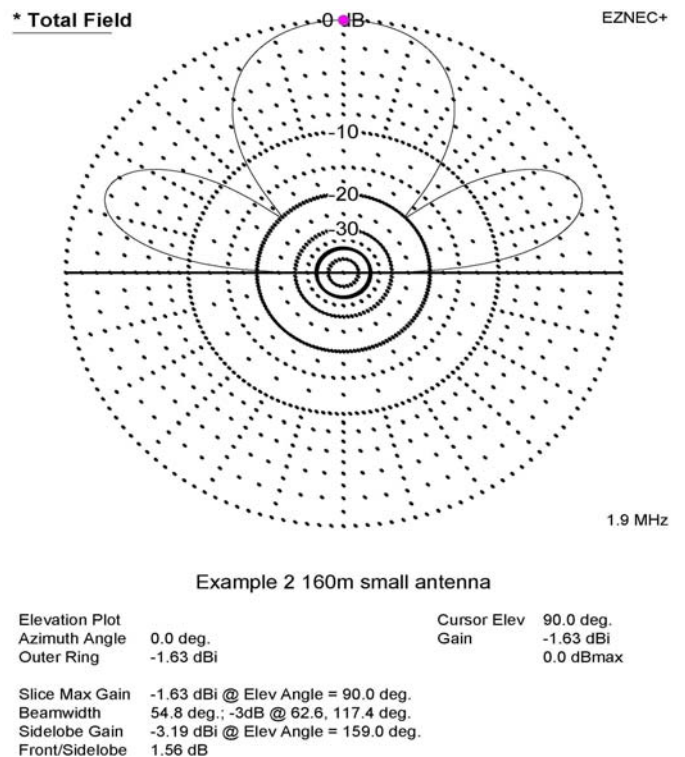
Fig. 7c. Example 2 $\varphi = 0°$, 80m height.

9

V. ANTENNA 3

The third example geometry is shown in Figure 8, and is an exercise in re-configuring Antenna 2 to give greater current vector alignment. In this case, the right "half-panel" of the Antenna 2 antenna is rotated up, so that the overall bounding geometry is no longer square.
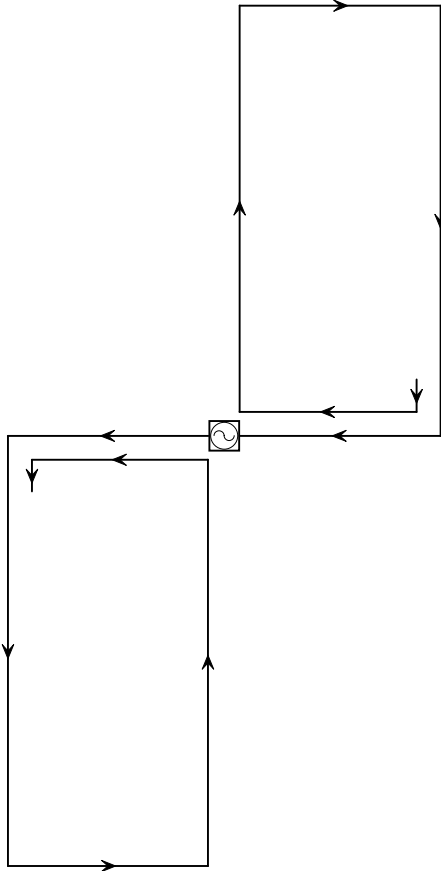
Fig. 8. Example 3 configuration.

This antenna geometry, with a wire diameter of 2 mm and height (of the antenna's bottom) above ground of 1 meter gives a resonant frequency close to 1.9 MHz with a feed-point impedance of $13 - j24\ \Omega$. Total wire length is again about 73 meters. This configuration is more awkward to implement, as each of the two antenna "panels" are 15 feet wide by 30 feet tall, so there is the mechanical complication that the overall height is some 60 feet, and the two panels do not sit one on top of the other vertically. Nonetheless, it is a logical re-arrangement of the Antenna 2 antenna to further increase current vector alignment. The improved feed-point impedance is encouraging, and the three elevation plots corresponding to the earlier cases are presented below in Figure 9a-c. As before, the antenna bottom is 1 meter above real ground with $\sigma = 3$ mS/m and $\epsilon_r = 12$ in Figure 9a-b, with the diffence in Figure 9c being that the antenna has been elevated to 80 meters above ground.

Fig. 9a. Example 3 $\varphi = 0°$ elevation plot.

Fig. 9b. Example 3 $\varphi = 90°$ elevation plot.

* Total Field — 0 dB — EZNEC+

1.9 MHz

160m opened spirals

Elevation Plot	Cursor Elev	40.0 deg.
Azimuth Angle 0.0 deg.	Gain	-1.59 dBi
Outer Ring -1.59 dBi		0.0 dBmax

Slice Max Gain   -1.59 dBi @ Elev Angle = 40.0 deg.
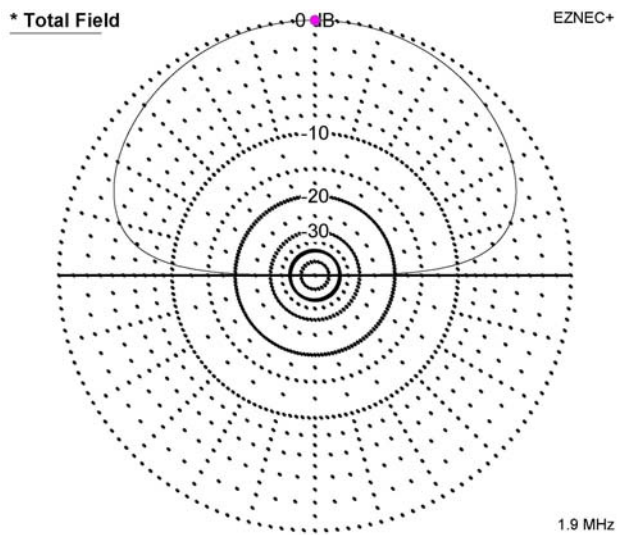Beamwidth   55.9 deg.; -3dB @ 7.6, 63.5 deg.
Sidelobe Gain   -1.59 dBi @ Elev Angle = 140.0 deg.
Front/Sidelobe   0.0 dB

Fig. 9c. Example 3 $\varphi = 0°$, 80m height.

VI. Wire Diameter

It should be noted that the diameter chosen for the antenna wire has a significant effect on the antenna feed-point impedance, resonant frequency, and efficiency. To illustrate the effect, the table below contains the results for various diameters in the case of Antenna 2 at height 1 m above real ground. The tabulated feed-point impedances are at resonance, which decreases about 400 kHz through the 160m band as the wire diameter increases from 0.05 mm to 25 mm. Recall that copper conductor loss has been included in all the numerical modeling runs.

Wire Diam.	Feed-point Z	Max. Gain ($\varphi = 0°$)
0.05 mm	$392 + j10 \ \Omega$	-21.6 dBi
0.25 mm	$29 + j48 \ \Omega$	-10.4 dBi
1 mm	$9 - j21 \ \Omega$	-5.76 dBi
5 mm	$5 - j2 \ \Omega$	-3.37 dBi
25 mm	$4 + j23 \ \Omega$	-3.5 dBi

The trend is clearly illustrated. Namely, increased wire diameter gives a more efficient antenna, but the improved maximum gain assumes that full power can still be transferred into the antenna while the feed-point impedance is simultaneously moving in a direction that makes full power transfer more and more difficult to achieve.

A general conclusion from multiple case studies is that a minimum wire diameter of 1 mm is necessary for acceptable antenna efficiency. Since a wire diameter of 0.08" (a readily available electrical wire size, #12) corresponds to 2 mm, it is not hard to comply with minimum efficiency expectations.

VII. Concluding Remarks

The three example antennas discussed here all demonstrate that the best wire geometry for a given rectangular size limit that will produce a natural resonance at the 160m amateur band (or other frequency of interest, for that matter) with the least overall wire length remains to be discovered. Antennas 1 -3 are all superior to the touted Hilbert fractal dipole in this regard.

Comparing "apples to apples" by looking at feed-point impedances and maximum gain for a wire diameter of 2 mm for all three example antennas allows some useful practical comparisons. First, it is noteworthy that a characteristic they share is that maximum gain broadside to the plane of the antenna barely depends on height above ground. The elevation pattern plot changes qualitatively as each is elevated to 80 m above ground, but the maximum gain is essentially unchanged from that with t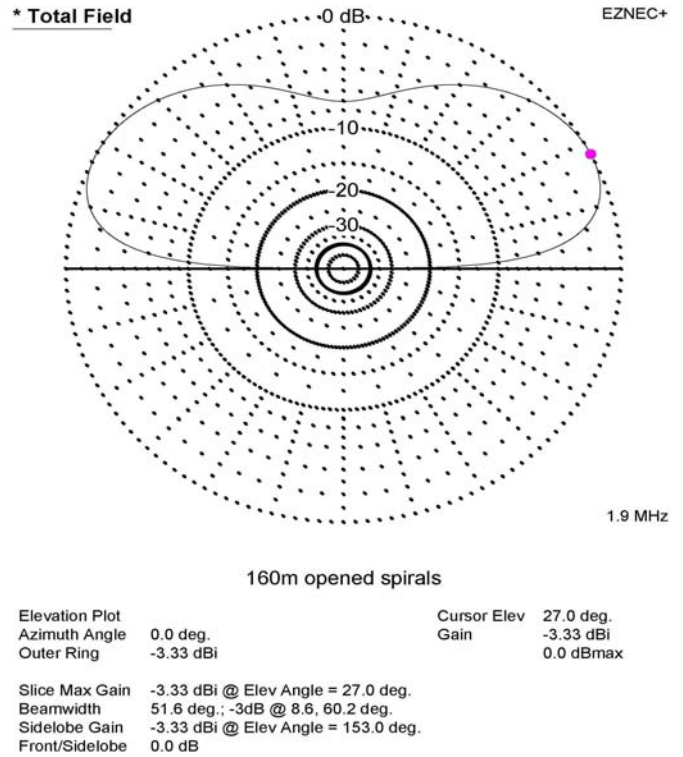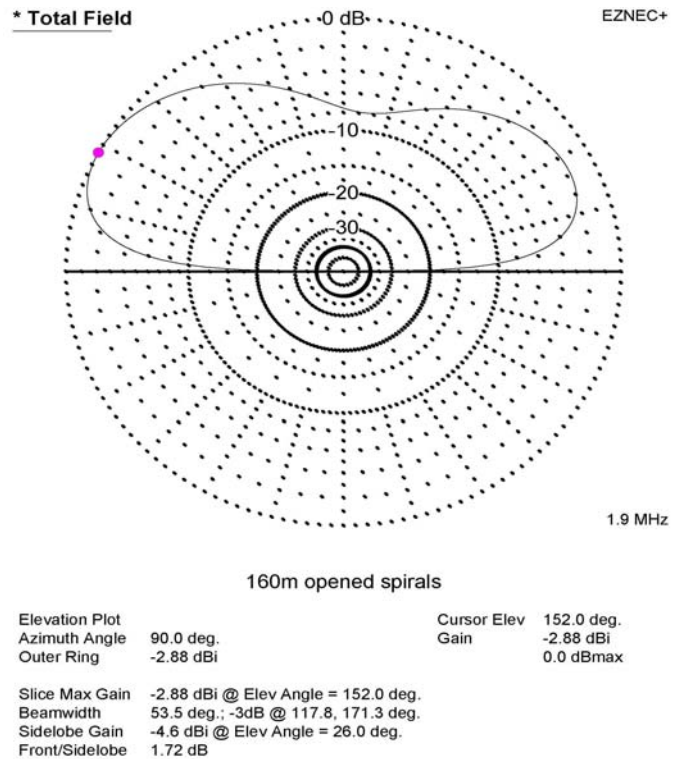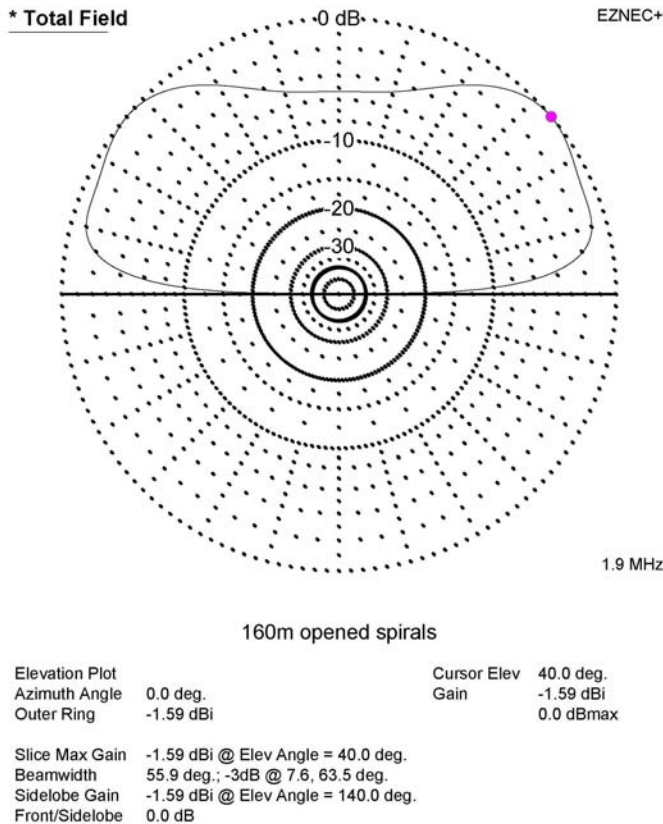he antenna bottom only 1 m above ground. The example antennas all are more "cloud burners" with high-angle radiation when mounted close to ground, but high angle radiation is widely desired among a large segment of the amateur radio community for 160m and 75m operation so, to many, this is actually an attribute.

Antenna 1 is the most compact, measuring slightly less than 20 feet on a side. However, its maximum gain is approximately -10 dBi, which is almost two full S-units (1 S unit = 6 dB) down from the 2.15 dBi gain of a half-wave dipole in free space. Probably this is more sacrifice in radiation efficiency than most users would be willing to accept. Antenna 2 is larger, at approximately 30 feet on a side, but is only one S-unit down from the full sized dipole. Given that the antenna can be mounted at ground level, this makes it an attractive possibility. The radiation resistance of Antenna 3 is twice that of Antenna 2 and it has a maximum gain about 1.5 dB greater. The disadvantages of Antenna 3 are an awkward geometry for construction and deployment, and its overall height of 60 feet.

It would not be unreasonable to conclude that Antenna 2 is the best overall compromise antenna of the lot.

Readers are invited and encouraged to devise and analyze their own alternative designs, taking current vector alignment into consideration as new geometries are conceptualized. The author would welcome any reports of progress and noteworthy successes.

Finally, the reader will note that references [3]-[7] are not associated with specific points or statements in the text of this article, which is somewhat unusual. They are included, however, as deserving mention and credit because their content is relevant to, and influenced, this paper. The author gratefully acknowledges inspiration for this engineering application study gained from the short course on advances in electrically

11

small antennas conducted by Steven Best at the 2004 IEEE International Symposium on Antennas and Propagation.

REFERENCES

[1] J. Anguera et al., "The Fractal Hilbert Monopole: A Two-Dimensional Wire," *Microwaveand Optical Tech. Lett.* **36**, 2102 (2003).

[2] EZNEC is a software product of Roy Lewallen, as described at http://www.eznec.com/.

[3] Best, S.R.and Morrow, J.D.,"The effectiveness of space-filling fractal geometry in lowering resonant frequency," *Antennas and Wireless Propagation Letters* , Volume: 1 , Issue: 5 , 2002, p 112 - 115.

[4] Vinoy, K.J., Jose, K.A., Varadan, V.K., and Varadan, V.V., "Resonant frequency of Hilbert curve fractal antennas," *Antennas and Propagation Society International Symposium*, 2001. IEEE , Volume: 3 , 8-13 July 2001, p 648 - 651.

[5] Xuan Chen, Safieddin Safavi Naeini, and Yaxin Liu, "A down-sized printed Hilbert antenna for UHF band," *Antennas and Propagation Society International Symposium*, 2003. IEEE , Volume: 2 , 22-27 June 2003, p 581 - 584.

[6] Best, S.R.and Morrow, J.D., "On the significance of current vector alignment in establishing the resonant frequency of small space-filling wire antennas," *Antennas and Wireless Propagation Letters* , Volume: 2 , Issue: 13 , 2003, p 201 - 204.

[7] Vinoy, K.J., Abraham, J.K., and Varadan, V.K., "Fractal dimension and frequency response of fractal shaped antennas," *Antennas and Propagation Society International Symposium*, 2003. IEEE , Volume: 4 , 22-27 June 2003, p 222 - 225.

A Finite Difference Time Domain Technique for the Simulation of Moving Objects

Matthew J. Inman, Atef Z. Elsherbeni, and Charles E. Smith
mjinman@olemiss.edu, atef@olemiss.edu,cesee@olemiss.edu

Department of Electrical Engineering
Center For Applied Electromagnetic Systems Research (CAESR)
The University of Mississippi

Abstract - Normally in the finite difference time domain (FDTD) technique, static objects are modeled in a time domain simulation as a field propagates around them, and possibly inside these objects. This paper illustrates a method in which EM fields and a moving object can be modeled using the FDTD technique. By using a technique of dielectric approximation and intermediate step field movement, it is possible to model the movement of objects by the FDTD technique. This paper illustrates these principles in a one-dimensional domain.

1. Introduction

The finite difference time domain technique is a well-known method for modeling Maxwell's equations in time. The technique divides the intended geometry into a spatial grid and solves for the electric and magnetic field components at discrete points. The material at each point on the spatial grid is characterized by its properties (permittivity, permeability, conductivity) in each of the Cartesian directions. From these material characteristics, the coefficients needed to update the fields at each time step can be computed. The technique used in this paper is derived from the algorithm defined by Yee [1]. This approach places all of the magnetic components one-half spatial step in front of the electric components, as well as computing the magnetic fields at one half time step after the electric fields.

In this example using a dielectric material, each spacial cell extends from one E_z point to the next. Component properties are calculated at these points and are used to update the appropriate fields. This spatial setup lends itself well to the approximations needed in order to simulate moving objects.

2. Physical Approximations

In FDTD the geometry is divided into a spatial mesh, which at each point on this mesh, has its own set of coefficients depending upon the material the point lies within. For example a point that lies solely within the interior of an object would have coefficients related to the conductivity and permittivity of that object. However, when the point represents the boundary of that object, the point is assigned an average of the properties of the two objects. Likewise if the object is a magnetic material, the same ideas would apply.

In order to model an object moving at a constant speed, the coefficients on the boundaries must be constantly updated as the object moves. On the forward boundary cell of the moving object, coefficients are modified at each step until it becomes an inside cell. Likewise on the back boundary cell, coefficients are modified at each step until it becomes free space (or the background material at that time). When the coefficients on the front and back edges have been modified until they are completely dielectric or free space, the boundaries have moved one spatial cell in the direction of movement as shown in Figure 1.

This is a simple example showing the fundamental approach. Characteristics such as conductivity can be approximated in the same way.

3. Field Approximations

Modifying the coefficients as the object moves provides a good foundation, however, it neglects the propensity of the fields to move with the object. This tendency of the fields to move depends directly on the material of the moving object itself. In order to model this, an assumption is made to separate the field in the region of the moving object. For non-magnetic material, only the E fields need to be split into two components, $E_{background}$ and E_{object}. The E_{object} is the portion that exists within the moving object and moves with it, such that:

$$E_{object} = E_{total} - E_{background} \qquad (1)$$

While E_{object} exists within the object itself, $E_{background}$ exists everywhere including inside of the object region. The two fields combined must be the same as the total field, these two fields can be related as:

13

$$E_{background} = \frac{1}{\varepsilon_r} E_{total} \quad (2a) \quad , \quad E_{object} = \frac{\varepsilon_r - 1}{\varepsilon_r} E_{total} \quad (2b)$$

By splitting the field into these two components, the contributions due to the moving field can be calculated. Then by re-interpolating the field at the grid points as it is moved, a better representation for the actual E field can be used for the updating of the H fields. The fields for E_{object} are shifted in space by the appropriate amount for one time step and are re-interpolated at the grid points. So that the total E field at time step n used when updating the H field becomes:

$$E_{total}^n = E_{background}^n + \left[\frac{E_{object}^n + E_{shifted-object}^n}{2} \right] \quad (3)$$

The averaging provides a good balance for what the E field is when updating H and what it will be when updating E at the next time step. The $E_{shifted-object}^n$ field at each grid point is calculated using a first order LaGrange approximation where m is the distance the object moves per time step.

$$E_{shifted-object_p}^n = \left(\frac{\Delta x - m}{\Delta x} \right) E_{object_p}^n + \left(\frac{m}{\Delta x} \right) E_{object_{p-1}}^n \quad (4)$$

This equation assumes movement in only one cardinal direction and in the direction of increasing index for the grid points (denoted by "p"). In a 2D or 3D environment the same equation would be applied to all components of E, separately.
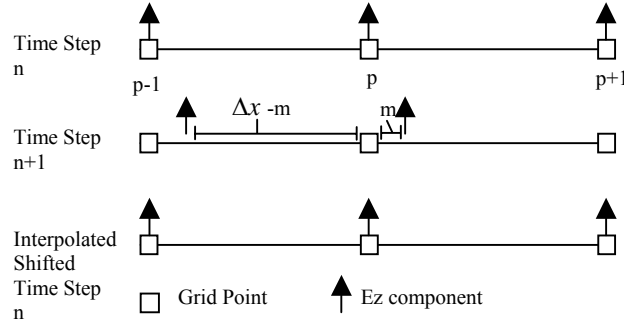
Figure 2. Interpolation of shifted fields.

Since all the materials in this paper are assumed to have a permeability of 1, it is not necessary to split or adjust the H fields inside the object. If the objects used contained materials with magnetic susceptibility ($\mu_r > 1$), a similar procedure to that outlined for the E fields and coefficients would be used.

4. Computational Implementation

Since the movement of the object is assumed to be constant, computational time can be saved by pre-calculating constants, such as the change per time step of each coefficient. With the object moving in one direction, only the coefficients at the front and rear boundaries of the object will change. By keeping track of where these boundaries are and knowing how much they change per time step, modification of the coefficient array becomes an almost trivial process. The standard 1D updating equations used here are [2]:

$$E_{zi}^{n+1} = Ceze(i)E_{zi}^n + Cezh(i)(H_{xi}^{n+\frac{1}{2}} - H_{xi-1}^{n+\frac{1}{2}}) \quad (5a) \qquad H_{xi}^{n+\frac{1}{2}} = Chxh(i)H_{xi}^{n-\frac{1}{2}} + Chxe(i)(E_{zi}^n - E_{zi-1}^n) \quad (5b)$$

For the background E field, no change in either of the updating equation coefficients is required for outside the object region. However, since the field in the region where object exists is represented by the combination of the object and background fields, a new set of coefficients is required for both fields. There are two coefficient arrays that have to be dealt with for the object E field, internal to the object. These coefficients at node "i" are given by:

$$Cezh = \frac{\Delta t}{\varepsilon_0 \left(\varepsilon_r + \frac{\Delta t \sigma_e}{2\varepsilon_0} \right) \Delta x} \quad (6a) \quad , \quad Ceze = \frac{\varepsilon_r - \frac{\Delta t \sigma_e}{2\varepsilon_0}}{\varepsilon_r + \frac{\Delta t \sigma_e}{2\varepsilon_0}} \frac{1}{\Delta x} \quad (6b)$$

In order to account for the split fields, E_{object} and $E_{background}$ will be updated separately. In these updating equations, the E field used is not the total field at that point, but rather the calculated object or background field at the same point in the last time step. Since there are two E fields, but only one H field, the H field used in the updating equations represents the total H field at the spatial location. Since we only need the H field contribution to either one of the split E fields, a second multiplier is added to the $Cezh$ coefficient to find its contribution to either E field. For $E_{background}$ this coefficient is 1 for all areas not containing the object. Likewise for the E_{object} field calculation, this coefficient is zero outside the object. For points inside the object this coefficient is a function of the object relative permittivity. For $E_{background}$ inside the object it is $(1/\varepsilon_r)$, and for E_{object} the coefficient becomes $(\varepsilon_r-1)/\varepsilon_r$.

On the forward and backward edges of the moving object the coefficients are not as straightforward. In order to model the object as it moves, dielectric coefficients are slowly built up and removed from the edges. The simplest way to implement this is to pre-calculate the differential change in the coefficients on the edges and simply add or subtract this amount from the appropriate places [3].

Once the object and background E fields are updated, the approximation (discussed in section 3) for the field as it moves can be calculated based on the splitting of the fields and the dielectric approximation. The formula given by (3,4) actually compresses or dilates the waves emanating from the object. This effect represents a Doppler shift in the reflected wave from the moving object.

The H field updating is performed to complete the cycle by using the coefficients at node "i" [2]:

$$Chxh = \frac{\mu_r - \dfrac{\Delta t \sigma_m}{2\mu_0}}{\mu_r + \dfrac{\Delta t \sigma_m}{2\mu_0}} \frac{1}{\Delta x} \quad (7a), \qquad Chxe = \frac{\Delta t}{\mu_0 \left(\mu_r + \dfrac{\Delta t \sigma_m}{2\mu_0} \right) \Delta x} \quad (7b)$$

The next additional step needed is the actual modification of the coefficients on the leading and trailing edges. This is done for both the object and background coefficient arrays due to movement during one time step. After an appropriate number of time steps, it is time to advance the location of the starting and stopping edges of the structure one cell in the direction of movement.

5. Results

In order to verify the proper operation of the method, several simple simulations were examined. For simplicity, the method was implemented in a one-dimensional FDTD code. The domain (shown in Figure 3) consisted of 3000 points with Δx of 0.1m. An object was defined from point 300 to point 700 and was programmed to move in the negative x direction. A plane wave was initially set up in the domain with the position of the leading edge of the Gaussian waveform at 150m and made to propagate towards the object. The total E field was sampled at a point close to the center. The time step used in the simulation was 300 ps in order to improve the stability of the system.

To prove that the technique works effectively, a simple system of measuring the Doppler shift of the reflected wave is used. The simulation excites the domain using a derivative of a Gaussian wave pulse. This type of pulse is used because of its smooth on and off operation and because it has a peak value at a non-zero frequency. By measuring the shift of this peak location, an estimate for the speed of the object can be calculated using a simple Doppler shift formula. As the speed of the object increases towards the speed of light, the relativistic Doppler formula (8) should be used for higher accuracy [4]. For the results shown, the relativistic Doppler formula was used.

$$\frac{\text{shift in wavelength}}{\text{wavelength}} = \sqrt{\frac{1 + \frac{V}{C}}{1 - \frac{V}{C}}} - 1 \quad (8)$$

Examining the simplest case of a perfectly conducting (PEC) object, the effects can be clearly seen. In order to model the object as a PEC, the coefficients for the object are calculated with a high electric conductivity. Through a process of 4 adaptive Fourier transforms, each increasing in resolution, the location of the respective peaks for the incident and reflected waves are located. Then using the Doppler shift formula and solving for the velocity (V), confirmation that the object is moving at the programmed speed can be provided. Figure 4 shows the relationship between the speed programmed in the simulation and the computed speed via Doppler shift for a moving conductor. The object was modeled as a conductor by assigning it a conductivity of 10^7 Siemens. The reference line refers to where the computed speed would be equal to the programmed speed. Some oscillation around the actual speed begins to happen as the speed decreases due to the finite maximal resolution of the discrete Fourier transform with the given time step. Because of this finite limit of resolution, this will set the lowest speed in which the object can be accurately modeled with the current FDTD simulation parameters.

15
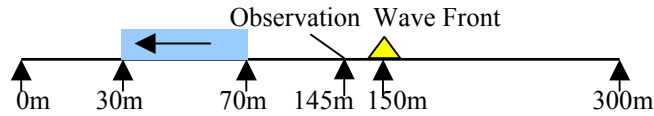
Figure 3. Domain configuration.

Running the same simulation again for a dielectric object with a relative permittivity of 7.2, as shown in Figure 5, similar results are observed. The measured Doppler shift agrees closely with the actual value in the upper range, while in the lower range below the limit defined by the resolution of the discrete Fourier transform it oscillates around the programmed reference velocity.

6. Conclusions

Through the use of this approach, it is possible to model moving objects using the FDTD technique. The use of both coefficient approximations and field movements to model both the movements effect on objects and on its related fields have proved its ability to predict expected results. There are still many subjects needing to be addressed for the analysis of the data in order to extend this concept to 2D and 3D FDTD analysis.
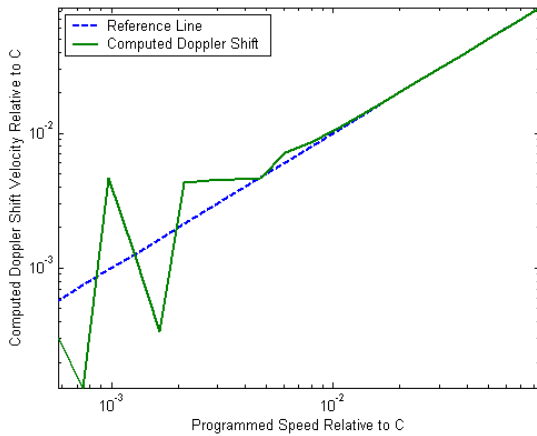
Figure 4. Computed Doppler shift of moving conductor.
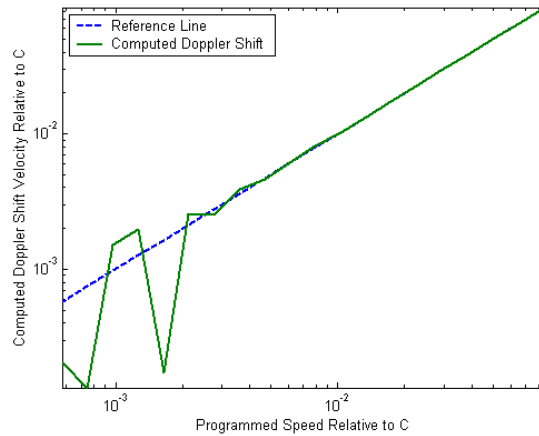
Figure 5. Computed Doppler shift of moving dielectric.

References

[1] K. S. Yee, "Numerical Solution of Initial Boundary Value Problems Involving Maxwell´s Equations in Isotropic Media", *IEEE Trans. Antennas and Propagation.* Vol. AP-14, S. 302-307, 1966.
[2] A. Z. Elsherbeni, "FDTD Course Notes", *Department of Electrical Engineering, The University of Mississippi,* MS, Spring 2001.
[3] M. J. Inman, A. Z. Elsherbeni, and C. E. Smith, "Finite Difference Time Domain Analysis of Moving Objects", *The 18th Annual Review of Progress in Applied Computational Electromagnetics,* ACES'02, Monterey, California, March 2002.
[4] Cornell Astronomy Doppler Notes, "Relativistic Doppler Shift", http://astrosun.tn.cornell.edu/courses/astro201/doppler_rel.htm .

Book Review
   By Dr. Ji Chen

Title: **Grid Computing For Electromagnetics**
by Luciano Tarricone, Alessandra Esposito
Hardcover: 266 page**s**
Publisher: Artech House Publishers (August 30, 2004)
ISBN: 1580537774

The design of advanced electronic systems, such as wireless products, often requires several iterations of prototyping. Due to the complex nature of these products, accurate electromagnetic (EM) modeling/simulations have become necessary. However, most EM simulation tools are very CPU intensive. Often time, simulation time may go beyond one day. This makes some modeling/simulation tools not very applicable for practical designs.

With the recent advancement in parallel computing, it is now feasible to use "supercomputer" to alleviate such CPU intensive simulations. Among various parallel computing approaches, two distinct methods for computational electromagnetic society are the Open specifications for Multi Processing (OpenMP) based scheme and the message passing interface (MPI) based technique. Each paradigm has its own advantages and disadvantages. For practical electromagnetic simulations, it comes down to the affordability of computer platform vs high performance computing. In terms of Gflops per dollar, the MPI based approach typically has a clear advantage. For example, eight-node OpenMP UNIX workstations could cost around $100K, while an eight-node LINUX cluster, with similar performance and comparable amount of memory, can be assembled under $10K. Furthermore, if one can use available computer resources across the Internet, the cost for MPI computing will be even lower.

"Grid computing for electromagnetics" is one of the first books that give the background, implementation, and examples on how to develop your own parallel electromagnetic designs on grid environment. It is a book on parallel computing and beyond. It starts with the parallel high performance computing (HPC) and goes beyond it by introducing cooperative engineering and real time data management on grid environment. The core of this book is Chapters 4-6 where three EM applications, viz the parallel MPI finite-difference time-domain (FDTD) method, the cooperative CAE of rectangular aperture array antenna, and the planning, managing and monitoring of wireless radio base station network, are discussed under the GC framework. Before these applications are elaborated, the authors prepare the readers with some fundamental knowledge of GC by introducing what is a grid environment, explaining the enabling technologies and dedicated tools related to the GC, and describing a step-by-step procedure on how to build you own cluster in Chapters 1-3. Although Chapters 1-3 may not be interested to some researchers who have excellent computer administrative support, it is still recommended that readers go through these chapters since understanding the limitations of the grid environment will help us to design better scalable GC algorithms.

This book consists of seven chapters and four appendixes. The four appendixes describe some required knowledge related to GC. These include basics of UNIX/LINUX operating systems, some foundations of cryptography and security for grid environment, and some fundamental electromagnetics related to the examples in the books.

Chapter 1 covers the general concepts of grids for GC. Parallel and distributed programming are first reviewed. The web computing is then introduced and followed by the definition of computational grids, where both hardware and software facilities can be heterogeneous. This is a distinct difference between the GC and most current parallel computing platforms, where nodes are often unitary in terms of both software and hardware. Standard three-layer architecture is introduced guarantee smooth communications between different computer platforms.

To enable GC, enabling technologies and dedicated tools are described in Chapter 2. Objects orientation software designs concepts are first described. To enable GC on heterogeneous computer platforms, the grid middleware must be used. In particular, the book describes the Globus Toolkit (GT), one of such tools that enable the secured communications between different nodes on the grid environment. After a detailed description of the Globus Toolkit, the MPICH-G2, a MPI in grid environment based on GT is discussed. The MPICH-G2 allow users to couple multiple machines belong to the same grid for MPI applications.

In Chapter 3, the step by step procedure of setting up grid for GC is introduced. Following this procedure, readers, with some help from computer system administrator, should be able to set up his/her grid environment. The GT is used as the standard in this book and the set up details for the MPICH-G2 on grid environment is also provided.

Chapter 4 focuses on the implementation of the MPI FDTD in grid environments. After reviewing fundamentals of the FDTD method, the authors describe the MPI FDTD implementation. As expected, several barriers need to be inserted in the MPI FDTD implementation to synchronize the operations of processes. Considering the fact that each node on the grid can be heterogeneous, additional steps, such as installing of MPICH-G2 library at each node, copying and compiling source code at each node must be performed prior to MPI simulations. With these detailed set up procedure and software provided in the attached CD-ROM, readers are ready to explore the MPI FDTD code on a grid environment! It should be noted that the load balance is not immediately discussed in the chapter. Since the performance of each node and the network traffic between different nodes can be quite different on a grid environment, it is crucial to have balanced workload (in terms of CPU execution time) for each node. Some load balance discussions are provided in the next chapter and it is not hard for readers to develop their own schemes to decompose the original computational workload among various nodes to achieve the maximum speed up.

Chapter 5 describes the CAE of flange-mounted rectangular apertures using GC. Rather than repeating parallel implementations of numerical techniques, the emphasis hers is on the cooperative engineering, where multi-tasks are handled in the grid environment. This is beyond the traditional parallel computing where the goal is to reduce the CPU time of a single software package. Cooperative engineering allows each node has its own electromagnetic module related to a specified task of the entire design, GC will provide the common protocol that allows the smooth interaction among various nodes towards the whole system design.

Chapter 6 further discusses the real time data communication and management in the GC for wireless radio base station networks. The integrated system for network optimum planning (ISNOP) is used as an example and how to implement it in GC is provided. This application demonstrates that in addition to its functions in high performance computing and cooperative engineering, the GC can also be used towards real-time management for

electromagnetic date produced by heterogeneous network of sources. In this application, the GT application programming interface is used for remote data access.

Overall, this is an interesting and practical book that gives the step by step instruction on how to build your first grid environment for electromagnetic applications. A CD-ROM, with necessary supporting software and some source codes, is attached at the end of the book. With some help from computer system administrator, one should be able to build up a simple five-node grid environment within one day and begin to explore the advantage of GC.

Ji Chen, Assistant Professor
Department of Electrical and Computer Engineering
University of Houston
4800 Calhoun Blvd.
Houston, TX 77204

2005 IEEE/ACES International Conference on Wireless Communications and Applied Computational Electromagnetics

3-7 April 2005
Hilton Hawaiian Village, Honolulu, Hawaii

Advanced Program

SHORT COURSES

April 3: 8:00 – 12:00 AM

1. *Principles of mobile communication viewed under a Maxwellian context*: Dr. Tapan K. Sarkar

2. *Neural networks and their applications to electromagnetic modeling*: Dr. Christos Christodoulou

3. *Diversity Combining in Fading Channels*: Dr. Lal Godara

4. *Dielectric resonator antenna, theory and design*: Dr. Ahmed Kishk

April 3: 1:00 – 5:00 PM

5. *Finite element method in time and frequency domains for solution of electromagnetic field problems*: Dr. Magdalena Salazar Palma

6. *Use of higher order basis in solution of electromagnetic field problems*: Dr. B. Kolundzija

7. *Application of genetic algorithms in electromagnetics*: Dr. Randy Haupt

8. *Antennas for wideband and phased array applications*: Dr. Ahmed Kishk and Dr. Atef Elsherbeni

TECHNICAL PROGRAM

April 4	8:00-11:20 AM	South Pacif
1	**Technologies for Ultra-Wideband Communication**	

8:00 Performance of Ultra-Wideband Transmission with Pulse Position Amplitude Modulation and RAKE Reception
Wei Li, T. Aaron Gulliver, Hao Zhang

8:20 Time Hopping QPSK Impulse Signal Transmission for Ultra Wideband Communication System in the Presence of Multipath Channel
Chaiyaporn Khemapatapan, Watit Benjapolakul, Kiyomichi Araki

8:40 Exploitation of Extra Diversity in UWB MB-OFDM System
Joo Heo, KyungHi Chang

9:00 Source Localization using Reflection Omission in the Near-Field
Ziba Ebrahimian, Robert A. Scholtz

9:20 Position localization with impulse ultra wide band
Guoping zhang

9:40 Coffee Break

10:00 Receiver Sites for Accurate Indoor Position Location Systems
Ziba Ebrahimian, Robert A. Scholtz

10:20 Characterization of the Ultra-Wide Band Channel
Feliziani Mauro, Graziosi Fabio, Santucci Fortunato, Di Renzo Marco, Manzi Giuliano

10:40 Design and Performance Analysis of a UWB Tracking System for Space Applications
Jianjun Ni, Richard Barton

11:00 UWB Sampler for Wireless Communications and Radar
Jeong-Woo Han, Cam Nguyen

April 4	8:00-11:40 AM	South Pacif
2	**Emerging Algorithms for MIMO Systems**	

8:00 Precodings for Transmission Rate Increasing for MIMO Single Carrier Block Transmissons
Shusuke Narieda, Katsumi Yamashita

8:20 Design of Synchronization Sequences in a MIMO Demonstration System
Guangqi Yang, Wei Hong, Haiming Wang, Nianzu Zhang

8:40 Compensation of Channel Information Error using First Order Extrapolation in Eigenbeam Space Division Multiplexing (E-SDM)
Toshihiko Nishimura, Takahiko Tsutsumi, Takeo Ohgane, Yasutaka Ogawa

9:00 Spatial Division Multiplexing of Space Time Block Codes for Single Carrier Block Transmission
Haiming Wang, Wei Hong, Xiqi Gao, Xiaohu You

9:20 Adaptive Channel Estimation for Multiple-Input Multiple-Output Frequency Domain Equalization
Xu Zhu, Fareq Malek, Yi Gong, Yi Huang

9:40 Coffee Break

10:00 On MIMO Signal Processing for Adaptive W-CDMA and OFDM Wireless Transceivers
Danijela Cabric, Dejan Markovic, Robert W. Brodersen

10:20 Performance Analysis of Adaptive Interleaving for MIMO-OFDM Systems
FengYe Hu, ShuXun Wang, Yang Liu

10:40 Adaptive MQAM Modulation for MIMO systems
Ramkumar Gowrishankar, M. Fatih Demirkol

11:00 Multiuser Detectors for MIMO DS/CDMA Systems
Fang-Biau Ueng, Shang-Chun Tsai, Jun-Da Chen

11:20 The Joint Space-Time Signal Detection Algorithm for MIMO DS-CDMA Systems with Multipath Fading Channels
Yung-Yi Wang, Jiunn-Tsair Chen, Ying Lu

8:00   Analysis of Dipole Antenna Printed on Thin Film by using Electromagnetic Simulators
Mitsuo Taguchi, Yuki Matsunaga

8:20   Electrically Large Structure in WIPL-D -- Scatterring Simulation of an Airplane
Mengtao Yuan, Tapan K. Sarkar

8:40   Into the Twilight Zone: How Does WIPL-D Perform in Quasistatics?
Ari Sihvola, Tapan Sarkar, Branko Kolundzija

9:00   Extended Limits of WIPL-D on PCs
Drazen S. Sumic, Branko M. Kolundzija

9:20   Efficient Analysis of Microwave Devices Based on Polygonal Modeling and WIPL-D Numerical Engine
Miodrag Tasic, Branko Kolundzija

9:40   **Coffee Break**

10:00   Equalization of Numerically Calculated Element Patterns for Root-Based Direction Finding Algorithms
Hossam A. Abdallah, Wasyl Wasylkiwskyj, Ivica Kopriva

10:20   WIPL-D Parallelization Effort
Christopher Card

10:40   Beta Test Analysis of WIPL-DP
Saad N. Tabet, Christopher Card

11:00   WIPL-D Results and Time Domain Response for an Impulse Radiating Antenna (IRA)
Mary C. Taylor, Tapan K. Sarkar

11:20   Deep Ground Penetrating Radar (GPR) – WIPL-D Models of Buried Sub-Surface Radiators
John Norgard, Michael Wicks, Randy Musselman

11:40   High Performance Low Cost Ferroelectric Phase Shifters Designed for Simple Biasing
Wayne Kim, Magdy Iskander

8:00   "Introduction to Antennas" – An Antenna Training DVD
Alan Nott. BEE CEng, MIEE

8:20   Shielding Effectiveness of Three Dimensional Gratings using the Periodic FDTD Technique and CPML Absorbing
J. Alan Roden, J. Paul Skinner

8:40   Hybrid Parallel Finite Difference Time Domain Simulation of Nanoscale Optical Phenomena
M. C. Hughes, M. A. Stuchly

9:00   A Comparative Study of RCS Computation Codes
CHIA, Tse Tong, ANG, Teng Wah, LIM, Kheng Hwee, DavidROWSE, Matthew AMOS

9:20   Modeling an HF NVIS Towel-Bar Antenna on a Coast Guard Patrol Boat - A Comparison of WIPL-D and the Numerical

Electromagnetics Code (NEC)
Darla Mora, Christopher Weiser, Michael McKaughan

9:40   **Coffee Break**

10:00   Modeling Multiple HF Antennas on the C-130/Hercules Aircraft - Part II
Stanley J. Kubina, Christopher W. Trueman, David Gaudine, Anita Ka Ki Lau

10:20   Modeling Antennas on Automobiles in the VHF and UHF Frequency Bands, Comparisons of Predictions and
Nicholas DeMinco

10:40   FDTD Analysis of a New Leaky Traveling Wave Antenna
G. M. Zelinski, M. L. Hastriter, M. J. Havrilla, J. S. Radcliffe, G. A. Thiele

11:00   Optimization of Aperiodic Waveguide Mode Converters
G. J. Burke, D. A. White, C. A. Thompson

11:20   Analysis, Design and Fabrication of Centimeter-Wave Dielectric Fresnel Zone Plate Lens and Reflector
Ali Mahmoudi

11:40   A Generalized MATLAB-based Distributed-computing Optimization Tool
Keith A. Lysiak, Jason Polendo

1:20   Wideband Printed Lotus Antenna
Abdelnasser Edek, Atef Elsherbeni, Charles Smith

1:40   Comparative Study of Wideband Properties of Planar Solid and Strip Fractal Bow-Tie Dipoles
Andrey S. Andrenko

2:00   Planar Elliptical Monopole Fed with CPW for UWB Applications
Kenneth C L Chan, Yi Huang, Xu Zhu

2:20   Techniques to Improve Ultra Wide Band Performance of Planar Monopole Antenna
X. N. Qiu, H. M. Chiu, A. S. Mohan

2:40   Design and Fabrication of a Multi-purpose Planar Antenna
Seong-il Park, Hyeon-Jin Lee, Yeong-seog Lim

3:00   **Coffee Break**

3:20   A Frequency-Selectable Patch Antenna of Circular Polarization with Integrated MEMS Switches
Sunan Liu, Ming-Jer Lee, G.-P. Li, Mark Bachman, FrancoDe Flaviis

3:40   Short Electromagnetic Pulse Probe Fed by Tow-Coaxial Balun: Sensitivity and Bandwidth Examining
Esrafil Jedari, Mohammad Hakkak, Majid Okhovvat, Alireza Foroozesh

4:00   A UWB Antenna with a Stop-band Notch in the 5-GHz WLAN band
Seong-Youp Suh, Warren L. Stutzman, William A. Davis, Alan E. Waltho, Kirk W. Skeba, Jeff L. Schiffer

4:20   Broadband Microstrip-Fed Modified Quasi-Yagi Antenna
Shih-Yuan Chen, Powen Hsu

4:40   Slot Antenna for Ultra Wideband System

Kamya Yekeh Yazdandoost, Ryuji Kohno

1:20 Enhanced MVDR Beamforming Implementation with Arbitrary Linear Arrays on DS/CDMA

KyungSeok Kim, Yong-Seok Choi, Chang-Joo Kim, Ik-Guen Choi

1:40 A Broadband Dual Circularly Polarized High Gain Microstrip Array

Weiping Dou, Dan Degutis

2:00 Development of Wideband Random Phased Arrays Composed of Modified Canted Sector Antennas

J. T. Bernhard, G. Cung, K. C. Kerby, P. E. Mayes

2:20 Low-cost Nonplanar Microstrip-line Ferrite Phase Shifter Utilizing Circular Polarization

Magdy F. Iskander, Jodie M. Bell, William W.G. Hui, Jar J. Lee

2:40 Active Frequency Selective Surfaces for Antenna Applications Electronically to Control Phase Distribution and Reflective/Transmissive Amplification

Peter Edenhofer

3:00 **Coffee Break**

3:20 Thinned Interleaved Linear Arrays

Randy Haupt

3:40 Lattice Spacing Effect on Scan Loss for Bat-Wing Phased Array Antennas

Thinh Q. Ho, Charles A. Hewett, Lilton N. Hunt

4:00 Phased Array for Limited Coverage

Howard Luh

4:20 Wireless Communication Applications of the Continuous Transverse Stub (CTS) Array at Microwave and Millimeter Wave Frequencies

William Henderson, William Milroy

4:40 Low Cost Compact Active Integrated Antenna with a Reactive Impedance Surface

Fabio Urbani, Filiberto Bilotti, Andrea Alù, Lucio Vegni

5:00 CFDTD Solution For Large Waveguide Slot Arrays

T. Ho, C. Hewett, L. Hunt, T. Ready, M. Baugher/K. Mikoleit

1:20 Numerical Dispersion of the 2-D ADI-FDTD Method

Qing-xin CHU , Lin-nian Wang , Zhi-hui Chen

1:40 A Novel HE-Coupling for Explicit Multigrid-FDTD

Peter Chow, Takashi Yamagajo, Tetsuyuki Kubota, Takefumi Namiki

2:00 New FDTD Model for Excitation of Microstrip Lines

Mikko Kärkkäinen

2:20 FVTD Simulations of Archimedean Spiral Antennas on Thin Substrates in Planar and Conformal Configurations

Christophe Fumeaux, Dirk Baumann, Rüdiger Vahldieck

2:40 Practical Considerations in the MRTD Modeling of Microwave Structures

Nathan Bushyager, Manos Tentzeris

3:00 **Coffee Break**

3:20 A Multiresolution Model of Transient Microwave Signals in Dispersive Chiral Media

I. Barba, A. Grande, A.C.L. Cabeceira, J. Represa

3:40 Modeling of Ground-Penetrating Radar for Detecting Buried Objects in Dispersive Soils

Konstantinos P. Prokopidis, Theodoros D. Tsiboukis

4:00 Advances in the Adjoint Variable Method for Time-Domain Transmission Line Modeling

Peter A. W. Basl, Mohamed H. Bakr, Natalia K. Nikolova

4:20 A Comparison of Marching-on-in-Time Method with Marching-on-in-Degree Method for the TD-EFIE Solver

Zhong Ji, Tapan K. Sarkar, Baek Ho Jung, Magdalena Salazar-Palma, Mengtao Yuan

4:40 Lightning Electromagnetic Fields Computation using Time Domain Finite Element Method

Glássio Costa de Miranda, Evandro José Ribeiro

1:20 An Integral Equation Method for the Scattering from Multiple Multilayered cylinders

Fad Seydou

1:40 A New Integral Equation for the Calculation of the Internal Impedance of a Conductor

luc knockaert

2:00 The Effect of Integration Accuracy on the MoM VIE Solution for Dielectric Resonators

Shashank Kulkarni, Sergey Makarov

2:20 Bistatic Scattering from a PEMC (Perfect Electromagnetic Conducting) Sphere: Surface Integral Equation Approach

Ari Sihvola, Pasi Yla-Oijala, Ismo V. Lindell

2:40 2D MFIE Solution Improvement by Regularization

Clayton P. Davis, Karl F. Warnick

3:00 **Coffee Break**

3:20 Combined-Field Solution of Composite Geometries Involving Open and Closed Conducting Surfaces

Ozgur Ergul, Levent Gurel

3:40 Formulation of surface integral equations for metallic, dielectric and composite objects

Pasi Ylä-Oijala, Matti Taskinen

4:00 A Simple Extrapolation Method Based on Current for Rapid Frequency and Angle Sweep in Far-Field Calculation of an Integral Equation Algorithm

Cai-Cheng Lu

4:20 Fast Construction of Wavelet-Based Moment Matrices in Solving Thin-Wire Electric Field Integral Equations

Mr. Amir Geranmayeh, Prof. Rouzbeh Moini, Prof. S. H. Hesam Sadeghi

4:40 Eddy currents in a gradient coil, modeled by rings and

patches
J.M.B. Kroot, S.J.L van Eijndhoven, A.A.F. van de Ven

April 5	8:00-10:00 AM	South Pacific
9	**Plenary Session**	

April 5	10:20-12:00 AM	South Pacif
10	**Direction of Arrival Estimation**	

10:20   A Neural Blind Beamformer for Cyclostationary Signals

Li Hongsheng, He You , Yang Rijie

10:40   A Low Complexity Adaptive Algorithm for Tracking of Eigenspace-Based Two-Dimensional Directions of Arrival

Kuo-Hsiung Wu, Wen-Hsien Fang, Hsin-Jung Chen, Jiunn-Tsair Chen

11:00   Direction of Arrival (DOA) Estimation Using a Transformation Matrix Through Singular Value

Seunghyeon Hwang, T. K. Sarkar

11:20   Real Time Angle of Arrival Estimation for GSM Signals

Peter S. Wyckoff, John T. Keeler

11:40   Mutual Impedance of Receiving Array and Calibration Matrix for High-resolution DOA Estimation

Hiroyoshi Yamada, Yasutaka Ogawa, Yoshio Yamaguchi

April 5	10:20-12:00 AM	South Pacif
11	**Dielectric Resonator Antennas**	

10:20   Broadband Dielectric Resonator Antennas Excited by L-shaped Probe

Ahmed A. Kishk, Ricky Chair, Kai-Fong Lee

10:40   Wideband Dielectric Resonator Antenna with Parasitic Strip

Tso-Wei Li

11:00   Slot Fed Broadband Dielectric Resonator Antenna

Tso-Wei Li

11:20   Dual-frequency Dielectric Resonator Antenna with Inverse T-shape Parasitic Strip

Tso-Wei Li

11:40   FDTD Analysis of a Probe-Fed Dielectric Resonator Antenna in Rectangular Waveguide

Yizhe Zhang, Ahmed A. Kishk, Alexander B. Yakovlev, Allen W. Glisson

April 5	10:20-11:40 AM	South Pacif
12	**Electromagnetic Imaging**	

10:20   Numerical Modeling Interaction of RF Field in MRI with a Pregnant Female Model

M.L. Strydom, K. Caputa, M.A. Stuchly, P. Gowland

10:40   Microwave Imaging of Three-Dimensional Dielectric

Objects Employing Evolution Strategies

Payam Rashidi, Magda El-Shenawee, Demetrio Macías, Eric Miller

11:00   Identification of Particles in Complex Structures from Scattering Data

Fad Seydou

11:20   Eccentric Annular Slot Antenna for Breast Cancer Detection Based on the Finite-Difference-Time-Domain

Vigneshware K. Raja, Magda El-Shenawee

April 5	10:20-12:00 AM	South Pacif
13	**Metamaterials**	

10:20   Time Domain Models of Negative Refractive Index Metamaterials

Wolfgang J. R. Hoefer, Poman P. M. So

10:40   Spectral Analysis of Negative Refractive Index Metamaterials Utilizing Signal Processing Techniques and Time-Domain Simulations

Titos Kokkinos, Raviraj S. Adve, Costas D. Sarris

11:00   Modeling of Metamaterial Structures Using an Extended FDTD Approach

Suzanne Erickson, Joshua Wong, Titos Kokkinos, Costas D. Sarris

11:20   Microwave/Millimeter Wave Metamaterial Development Using the Design of Experiments Technique

Daniela Staiculescu, Nathan Bushyager, Manos Tentzeris

11:40   Characterization of Meta-Material Using Computational Electromagnetic Methods

Manohar D. Deshpande, Joon Shin

April 5	1:20-4:00 PM	South Pacif
14	**Special Session: Technology for Emerging Commercial Millimeter-Wave Application**	

1:20   Technology for Emerging Commercial Applications at Millimeter-Wave Frequencies

Rudy Emrick, Steve Franson, Bruce Bosco, John Holmes, Steve Rockwell

1:40   High Performance SiGe BiCMOS Technology

Marco Racanelli, Sorin Voinegescu, Paul Kempf

2:00   Multi-Gigabit Wireless Test Bed at Millimetre Waves

Oya Sevimli, Val Dyadyuk, David Abbott,, Leigh Stokes, Stephanie Smith, John Arch, Mei Shen, Rod Kendall, Juan Tello

2:20   High Speed Data Communications based on W-band Automotive Radar MMIC

Carsten Metz, Torben Baras

2:40   Complementary Market Opportunites for Commercial & Military mm-Wave MMIC Devices

Roberto W. Alm

3:00   **Coffee Break**

3:20   Circuit and Module Challenges for 60 GHz Gb/s Radio

Joy Laskar

23

3:40   A Millimeter-Wave Multifunction Sensor for Wireless Monitoring of Displacement and Velocity

Seoktae Kim, Cam Nguyen

April 5	1:20-5:00 PM	South Pacif
15	**MIMO and Diversity System Characterization**	

1:20   Simulations of Diversity Gains of Multiple Omni and Directive Antennas in Rician Channel with varying K-

Marin S. Stoytchev, David C. Wittwer

1:40   Deterministic Channel Modeling and Performance of Monopolarized and Multipolarized MIMO Wireless Channels

Nuttapol Prayongpun, Kosai Raoof

2:00   Evaluation of Propagation Characteristics in Indoor Environment for MIMO System

Hidetoshi Chiba, Yoshio Inasawa, Yoshihiko Konishi, Shigeru Makino

2:20   On the Channel Capacity in MIMO Systems for Aeronautical Channels

Farid Ghanem, Gilles Delisle, Tayeb Denidni, Khalida Ghanem

2:40   Alamouti and Differential Transmit Diversity for Air-to-Ground Communications

Michael A. Jensen, Michael D. Rice

3:00   **Coffee Break**

3:20   Statistical Modeling of Site-specific Indoor Channels in Wireless Communications

Chan-Ping Lim, John L. Volakis, Kubilay Sertel, Rickie W. Kindt, Achilleas Anastasopoulos

3:40   On the Diversity Gain Using a Butler Matrix in Fading MIMO Environments

Alfred Grau, Jordi Romeu, Franco De Flaviis

4:00   Space-Polarization Diversity for a 2x2 MIMO using Space Time Block Codes

Nour Mohammad MURAD, David CARSENAT, Bernard JECKO

4:20   Performance of 2x2 MIMO Spatial Multiplexing in Indoor Environments

Yasutaka Ogawa, Hiroshi Nishimoto, Toshihiko Nishimura, Takeo Ohgane

4:40   A Transmit Antenna Selection Diversity Scheme for Wireless Communications

Jiaen Li, Myoung Seob Lim

April 5	1:20-5:00 PM	South Pacif
16	**Special Session: Electromagnetic Modeling by FEKO**	

1:20   A Computer Simulation of 400 MHz and 1000 MHz Antennas Located on a High Mobility Multi-Wheeled

Keith Anthony Snyder

1:40   Design and Analysis of a Pattern Selectable Airborne HF Antenna

Nathan P. Cummings

2:00   Hybrid Simulation of Electrically Large Millimeter-Wave Antennas

Steven J. Franson

2:20   Loop-Dipole Antenna Modeling using the FEKO Code

Wendy Lippincott, Tom Pickard, Randy Nichols

2:40   Fast Multipole Solution of Metallic and Dielectric Scattering Problems in FEKO

Johannes J van Tonder, Ulrich Jakobus

3:00   **Coffee Break**

3:20   A Horn-Fed Reflector Optimized with a Genetic Algorithm

Randy Haupt

3:40   Prediction of VHF Radiation Patterns on Gulfstream Aircraft

Christopher Penwell

4:00   Database Generation of Bistatic Ground Target Signatures

Amit Kumar Mishra, Bernard Mulgrew

4:20   Analysis of a Narrow Slot backed by a Rectangular Cavity using FEKO

Vivek Ramani, C. J. Reddy, Anthony Q. Martin

April 5	1:20-3:20 PM	South Pacif
17	**Low Frequency Electromagnetic Applications**	

1:20   Motional Eddy Currents Analysis in moving solid iron using magnetic equivalent circuits method

Mojtaba Mirsalim, Mehran Mirzayee, Igor A. Tsukerman

1:40   Analysis of a High-Speed Solid Rotor Induction Motor Using Coupled Analytical method and Reluctance Networks

Mehran Mirzayee, Hasan Mehrjerdi, Igor Tsurkerman

2:00   Electrostatic and Magnetostatic Finite-Difference Analysis without the 'Staircase' Effect

Igor Tsukerman

2:20   The Analysis of the Additional Substance Influence on the Grounding Grid Parameters by FEM

Anton Habjaniè, Mladen Trlep

2:40   Low-Frequency EM Field Penetration Through Magnetic and Conducting Cylindrical Shields

Michael A. Morgan

3:00   Electrodynamics of Dipolar Beads in an Electrophoretic Spherical Cavity

Meng H. Lean, Armin R. Volkel

April 5	3:40-5:00 PM	South Pacif
18	**Asymptotic and High Frequency Techniques**	

3:40   Multiscale Analysis of Panel Gaps in the Haystack Parabolic Reflector

Nader Farahat, Raj Mittra

4:00   Vectorial GO and Diffraction Decomposition of Physical Optics Scattering of Dipole Wave from Planar Surfaces in Terms of Modified Edge Representation Line Integrals

Luis Rodriguez, Ken-ichi Sakina, Makoto Ando

4:20	Efficient Macromodeling for Systems Characterized by Sampled Data
	rong gao

4:40	A High-Frequency Asymptotic Formulation for Temporal Characterization of Reflector Antennas
	Cassio Goncalves do Rego, Flavio Jose Vieira Hasselmann, Sandro Trindade Mordente Goncalves, Elias Lawrence Marques

---

April 6	8:00-11:40 AM	South Pacif
19	**Special Session: Communication Antenna Analysis and Design**	

8:00	Frequency Reconfigurable CPW-Fed Hybrid Folded Slot/Slot Dipole Antenna
	G. H. Huff, J. T. Bernhard

8:20	Modified Sierpinski Factal Antenna
	Tripti Luintel, Parveen Wahid

8:40	Parallel PSO/FDTD Algorithm for the Optimization of Patch Antennas and EBG Structures
	Nanbo Jin, Yahya Rahmat-Samii

9:00	Antennas and Propagation for Body Centric Wireless Communications
	A. Alomainy, P. S. Hall, Y. I. Nechayev, C. G. Parini, C. C. Constantinou

9:20	Calculation of SAR using FDTD sub-domain approach
	Tao Su, Raj Mittra, Wenhua Yu, Joe Wiart

9:40	**Coffee Break**

10:00	Narrow Beam Adaptive Array for Advanced Wireless Applications
	Meriam Rezk, Wayne Kim, Zhengqing Yun, Magdy Iskander

10:20	Neural Networks in Antenna Engineering - Beyond Black-Box Modeling
	Amalendu Patnaik, Dimitrios Anagnostou, Christos Christodoulou

10:40	Analysis of a Linear Slot Array Comprised of Tilted Edge Slots Cut in the Narrow Wall of a Rectangular Waveguide
	John C. Young, Jiro Hirokawa, Makoto Ando

11:00	Antennas for Distributed Nanosatellite Networks
	Thomas J. Mizuno, Justin D. Roque, Blaine T. Murakami, Lance K. Yoneshige, Grant S. Shiroma, Ryan Y. Miyamoto, Wayne A. Shiroma

11:20	A Coupled-Antenna Interrogator/Receiver for Retrodirective Crosslinks in a Distributed Nanosatellite
	Justin D. Roque, Stephen S. Sung, Blaine T. Murakami, Grant S. Shiroma, Ryan Y. Miyamoto, Wayne A. Shiroma

---

April 6	8:00-11:40 AM	South Pacif
20	**MIMO Systems**	

8:00	Development of RF Subsystems for MIMO and Beyond 3G Systems
	Jianhong Chen, Wei Hong, Jianyi Zhou , Jianing Zhao, Jianjun Wang

8:20	Applications of MIMO Techniques to Sensing of Cardiopulmonary Activity
	Dragan Samardzija, Olga Boric-Lubecke, Anders Host-Madsen, Victor M. Lubecke, Amy D. Droitcour

8:40	Modeling Front-End Signal Coupling in MIMO Systems
	Matthew L. Morris, Michael A. Jensen

9:00	Signal Enhancement in a Near-Field MIMO Environment Through Adaptivity on Transmit
	Seunghyeon Hwang, T. K. Sarkar

9:20	HSDPA Capacity Enhancement using MIMO in a Pico-cell Environment
	Pedro Vieira, Maria Paula Queluz, António Rodrigues

9:40	**Coffee Break**

10:00	Development of The MIMO System for Future Mobile Communications
	Wei Hong, Haiming Wang, Quangqi Yang, Nanzu Zhang, Jianyi Zhou

10:20	A Look at some of the Principles of Mobile Communication from a Maxwellian Viewpoint
	Tapan K. Sarkar

10:40	Performance of Space-Time Trellis Codes over Nakagami Fading Channels
	Mohammad O. Farooq, Wei Li, T. Aaron Gulliver

11:00	A New CDMA/SDMA Architecture with Transmit Diversity
	Wei Li, T. Aaron Gulliver

11:20	Feedback Equalization for MIMO systems
	Khalida Ghanem, Tayeb Denidni

April 6	8:00-12:00 AM	South Pacif
21	**Hybrid CEM Techniques**	

8:00	Parallel ICCG Solvers for a Finite-Element Eddy-Current Analysis on Heterogeneous Parallel Computation
	Takeshi Iwashita, Masaaki Shimasaki, Junwei Lu

8:20	Full Wave Analysis of RF Signal Attenuation in a Lossy Cave using a High Order Time Domain Vector Finite
	James Pingenot, Robert Rieben, Daniel White

8:40	Calculation of Polyphase Induction Motor Parameters Using Finite Element Method
	Reinaldo Shindo, Antônio Carlos Ferreira, George Alves Soares

9:00	A Highly Robust and Versatile Finite Element-Boundary Integral Hybrid Code for Scattering by BOR Objects
	Jian-Ming Jin

9:20	FE-BI Analysis of a Leaky-Wave Antenna with
	Leo Kempel, Stephen Schneider, Joshua Radcliffe, Dan Janning, Gary Thiele

9:40	**Coffee Break**

10:00	Nested Multigrid Finite Element Analyses of Eddy Current Losses in Power Transformers
	Erich Schmidt, Joachim Schoeberl, Peter Hamberger

10:20	Virtual Design of Insulation Elements Based on FEM and Automated Optimization Process
	Peter Kitak, Joze Pihler, Igor Ticar, Oszkár Bíró, Kurt

Preis

10:40   Application of an hp-adaptive FE method for computing electromagnetic scattering in the frequency domain

Niklas Sehlstedt, Adam Zdunek, Waldemar Rachowicz

11:00   Study of Electromagnetic Scattering form Material Object Doped Randomly With Thin Metallic Wires Using Finite Element Method

Manohar D. Deshpande

11:20   Acoustic Noise Signal Evaluation due to Magnetostrictive Effects in Electrical Equipment

Osama A. Mohammed, Nagy Y. Abed, Shreerang Ganu, Shuo Liu

11:40   Surface Based Differential Forms

James Pingenot, Chaunyi Yang, Vikram Jandhyala, NathanChampagne, Benjamin J. Fasenfest

---

April 6	8:00-12:00 AM	South Pacif
22	**Fast and Efficient CEM Methods**	

8:00   Two-Step Reduction Approach based on the Scattering-Symmetric Lanczos Algorithm for TLM-ROM

Dzianis Lukashevich, Andreas Cangellaris, Peter Russer

8:20   High-Throughput Transmission Line Matrix (HT-TLM) System in Grid Environment for the Analysis of Complex Electromagnetic Structures

Petr Lorenz, José Vagner Vital , Bruno Biscontini, Peter Russer

8:40   Fast Time Domain Integral Equation Solver for Dispersive Media with Auxiliary Green Functions

E. Bleszynski

9:00   Discontinuous Galerkin Time--domain Simulations for Electromagnetic Wave Propagation in Photonic Chrystals

Misun Min

9:20   Fast Adaptive Mode Reduction Scheme for Efficient Computation of Cascaded Filters by the MoL

Larissa Vietzorreck, Wilfrid Pascher

9:40   **Coffee Break**

10:00   FDTD Calculations using Graphical Processing Units

Matthew J. Inman, Atef Elsherbeni, Charles Smith

10:20   The FDFD with the Iterative Multi-Region Technique for the Scattering from Multiple Three Dimensional Objects

Mohamed Al Sharkawy, Veysel Demir, Atef Elsherbeni

10:40   Efficient Calculation of Field Distribution with High-Resolution Using Ray-Tracing Method

Zhengqing Yun, Magdy F. Iskander

11:00   Two-Level Preconditioning Techniques for Electromagnetic Wave Scattering Problems

Jeonghwa Lee, Jun Zhang, Cai-Cheng Lu

11:20   TM scattering from finite rectangular grooves in a conducting plane using overlapping T-block analysis

Yong Heui Cho

11:40   Adaptive Cross Approximation for MOM Matrix Fill for PC Problem Sizes to 157000 Unknowns

John Shaeffer, Francis Canning

April 6	1:20-5:20 PM	South Pacif
23	**Design and Analysis of Advanced Circuit Architectures**	

1:20   2D Coupled Electrostatic-Mechanical Model for Shunt-Capacitive MEMS Switch Based on Matlab Program

Ehab K. I. Hamad, Amr M. E. Safwat, Abbas S. Omar

1:40   Dynamic and Electrical Analysis of MEMS Capacitor with Accelerated Motion Effects

Kohei Kawano, Shafrida Shahrani, Takashi Mori, Michiko   Kuroda, Manos M. Tentzeris

2:00   Fast Full-Wave Analysis of Distributed MEMS Transmission Lines by the MoL

Wilfrid Pascher, Reinhold Pregla, Larissa Vietzorreck

2:20   Chip-Package Codesign of Receiver Front End Modules for RF/Wireless Applications

Yasar Amin, Prof. Hannu Tenhunen, Prof. Dr. Habibullah Jamal , Dr. Li-Rong Zheng , Xinzhong Duo

2:40   A Wide-band 0.5 um CMOS Low-Noise Amplifier

Ivy Lo, Derek Ah Yo, Ken Cheung, Victor M. Lubecke, Olga Boric-Lubecke

3:00   **Coffee Break**

3:20   Amplifier-Based Active Antenna Oscillator Design at 0.9-1.8 GHz

Isaac Waldron, Ayoob Ahmed, Sergey Makarov

3:40   Realization of a Sub-harmonic Mixer with a Substrate Integrated Waveguide Filter

Hongjun Tang , Yulin Zhang, Wei Hong

4:00   Synthesis of a dual-passband elliptic filter with equalized group delay

Juseop Lee, Man Seok Uhm, Jong Heung Park

4:20   Unilateral Amplifier S-Parameter Extraction Technique

Kendall S. Ching, Ryan Y. Miyamoto, Wayne A. Shiroma

4:40   Ultra-wideband Miniaturized Electromagnetic Bandgap Structures Embedded in Printed Circuit Boards: Theory, Modeling and Experimental Validation

Shahrooz Shahparnia, Omar M. Ramahi

5:00   Hybrid FDTD Analysis for Periodic On-Chip Terahertz (THz) Structures

Yasser A. Hussein, James E. Spencer

April 6	1:20-5:00 PM	South Pacif
24	**Propagation Channel Characterization**	

1:20   A Vectorial Analysis of UHF Propagation in a Three-dimensional Multislit Street Waveguide

Edgar Silva Júnior, Gilberto Arantes Carrijo

1:40   An Efficient Wave Propagation Model for Simulation and Analysis of Multipath Effects of Mobile Users in Indoor and Urban Environment

Steve Hall, Jei S. Chen, Shankar Venkatesan

2:00   A SBR Algorithm for Simple Indoor Propagation Estimation

Ryoichi Sato, Hiroshi Sato, Hiroshi Shirai

2:20	Propagation Prediction Software for Wireless Communication System Optimization
	Chad Takahashi, Zhengqing Yun, Magdy F. Iskander
2:40	Characterizing Dispersion in the Enclosed-Space Radio Channel using a Composite Mode Model
	J.P. Vant Hof, D.D. Stancil
3:00	**Coffee Break**
3:20	Measurements of a CW signal in Brazil and Comparison with Prediction using ITU-R P.1546-1
	A. J. Martins Soares, P. Carvalho
3:40	The Channel Characterization and Performance Evaluation of Mobile Communication Employing Stratospheric Platform
	Iskandar
4:00	Electromagnetic Propagation of Wireless Networks in Aircraft Cabins
	Mennatoallah Youssef, Linda Vahala, John Beggs
4:20	802.11ab Propagation Prediction Inside a B777
	Genevieve Hankins, Linda Vahala, John Beggs
4:40	Effect of Road Undulation on the Propagation Characteristics of Inter-Vehicle Communications in the
	Atsushi Yamamoto, Koichi Ogawa, Tetsuo Horimatsu, Katsuyoshi Sato, Masayuki Fujise

April 6	1:20-5:00 PM	South Paci
25	**Special Session: Recent Electromagnetics & Antennas Activities in the European Network "ACE"**	

1:20	European Effort Towards a Unified Framework for the Analysis of Antenna Structures
	G. A. E. Vandenbosch
1:40	Three Different Ways to Decorrelate Two Closely Spaced Monopoles for MIMO
	S. Dossche, S. Blanch, J. Romeu
2:00	FDTD Analysis of Reflectarray Radiating Cells
	Cadoret David, Laisné Alexandre, Marie-anne Milon, Gillard Raphaël, Legay Hervé
2:20	Built-in Multiband Antennas for Mobile Phone and WLAN Standards
	Cyril Luxey, Pascal Ciais, Georges Kossiavas, Robert Staraj
2:40	Multiscale Analysis of Array and Antenna Farm Problems
	L. Matekovits, A. Laza, F. Vipiana, P. Pirinoli, G. Vecchi
3:00	**Coffee Break**
3:20	Integral Equation Formulation for the Impedance Representation of Aperture-Coupled Devices with Finite
	Michael Mattes, Juan R. Mosig
3:40	A General Procedure to set up the Dyadic Green's Functionof Multilayer Conformal Structures and its Application to Microstrip Antennas
	Michael Thiel, Truong Vu Bang Giang, Achim Dreher
4:00	Binary Optical Mixing for Broadband THz Communication
	C. Sydlo, R. Mendis, J. Sigmund, M. Feiginov, H. L.

	Hartnagel and P. Meissner
4:20	Planar Terahertz Antenna Optimisation
	C. Sydlo, J. Sigmund, H.L. Hartnagel, R. Mendis, M. Feiginov and P. Meissner
4:40	EMANT: Integration of GiD and Kratos, Open and Flexible Computational Tools.
	Ruben Otin, Javier Mora, Eugenio Oñate

April 6	1:20-5:00 PM	South Paci
26	**Electromagnetic Analysis of Wave Phenomena**	

1:20	Time and Frequency Evolution of Precursor Fields in Dispersive Media using FDTD and Joint Time-Frequency
	Reza Safian, Costas Sarris, Mohammad Mojahedi
1:40	Multiple Scattering of Plane Electromagnetic Waves by two Dielectric Coated conducting strips
	Hassan A. Ragheb, Essam Hassan
2:00	Dipole Radiation in the Presence of a Planar Unidirectionally Conducting Screen
	Binhao Jiang
2:20	A New Method for Evaluation of Electromagnetic Field of Vertical Electric Dipole over Constant-impedance Plane
	Jiang Binhao, Liu Yongtan
2:40	A New Approach to Electromagnetic Wave Diffraction by Plane with an Impedance Discontinuity
	Binhao Jiang
3:00	**Coffee Break**
3:20	A New Computational Method for Plasmon Resonances of Nanoparticles and for Wave Propagation
	Igor Tsukerman
3:40	Far-Field RCS Prediction From Measured Near-Field Data Including Metal Ground Bounce
	Yoshio Inasawa, Shinji Kuroda, Shinichi Morita, Hitoshi Nishikawa, Yoshihiko Konishi
4:00	Analysis of Electromagnetic Field in Inhomogeneous Medium by Fourier Series Expansion Methods
	Tsuneki Yamasaki, Kastuji Isono, Takashi Hinata
4:20	Educational Software Package for Electromagnetic Scattering from Simple Two and Three Dimensional Canonical and Non-Canonical Objects
	Mohamed Al Sharkawy, Veysel Demir, Atef Elsherbeni
4:40	Hard and Soft Surfaces Realized by Frequency Selective Surfaces on a Grounded Dielectric Slab
	Manish Hiranandani, Alexander B. Yakovlev, Ahmed A. Kishk

April 7	8:00-12:00 AM	South Paci
27	**Integrated Antennas for Portable Devices**	

8:00	Dual-band Circularly Polarized Microstrip Antenna
	Tso-Wei Li
8:20	Multi-band Loop Antenna Integrated with a Telephone Handset

Muhammed Z Alam, Maria A. Stuchly

8:40   A Card-Type Inverted LFL Antenna for Dual-Frequency Operation

H. Nakano, K. Morishita, Y. Sato, H. Mimaki, J. Yamauchi

9:00   A Circularly Polarized Dual-Band Microstrip Antenna

Cyril Luxey, Fabien Ferrero, Gilles Jacquemod, Robert Staraj

9:20   Miniaturized, Wideband Fractal Patch Antenna

M.Jamshidifar, F.Arazm, Ch.Ghobadi, Javad .Nourinia,

9:40   **Coffee Break**

10:00   Meandered Planar Inverted-F Antenna for PCS Mobile Phone

Joo-Seong Jeon, Man-Hoe Heo, Jae-Won Noh

10:20   Coupled Retractable Whip/Stub Antennas for Mobile Phones

Faton Tefiku, Kevin Li

10:40   Development of Mobile Phone Using Dual-interface SIM and Fingerprint Recognition

Meihong Li

11:00   Analytical Calculation of Input Impedance of Rectangular Microstrip Patch Antennas on Finite Ground Planes

D. Chatterjee, E. Chettiar

11:20   A Study of Non-uniform Meandered and Fork-Type Grounded Antenna using iterative method.

Gharsallah ali, Zairi hsan, Glaoui mohamed

11:40   A Dual-Band Monopole Antenna for Mobile Communications

Yuehe Ge, Karu P. Esselle, Trevor S. Bird

April 7	8:00-10:40 AM	South Pacif
28	**Beamforming and Smart Antennas**	

8:00   New Constraints for Broadband Beamformers without Steering Delays

Lal C. Godara, M. R. Sayyah Jahromi

8:20   A New Implementation Approach for Cyclostationary Signal-Based Adaptive Arrays

Fang-Biau Ueng

8:40   Block Adaptive Beamforming via Parallel Projection Method

Wen-Hsien Fang, Sen-Hsien Hung, Kuo-Hsiung Wu

9:00   Steering Broadband Beamforming without Pre-steering

M. R. Sayyah Jahromi, Lal C. Godara

9:20   Phase-only Adaptive Processing based on the Direct Data Domain Least Squares Approach

Wonsuk Choi, Tapan K. Sarkar

9:40   **Coffee Break**

10:00   A New GSC-Based Adaptive Array

Fang-Biau Ueng

10:20   Performance Enhancement by Using Switch-Beam Smart Antenna in 802.11a WLAN System

Shao - Hua Chu, Hsin - Piao Lin, Ding - Bing Lin

April 7	8:00-12:00 AM	South Pacif
29	**System Architectures and Analysis**	

8:00   The Next Generation Air to Ground Communication System Using for Air Traffic Control

HO DAC TU

8:20   Novel Interpolator Structure for Digital Symbol Synchronisation

Markku Kiviranta

8:40   An Efficient Timing Synchronization Method for OFDMA System

JungJu Kim, Jungho Noh, KyungHi Chang

9:00   Improvement of Voice Activity Detection Algorithm Based on 3G Partnership Project

Zhang liang, Bian zhengzhong, Gao yingchun

9:20   Performance of Digital Transceiver for Space-Time Coded Cooperative Multihop Wireless Communication Systems

Pham Bao Thi Ngoc, Takaaki Zakoji, Hidekazu Murata, Kiyomichi Araki

9:40   **Coffee Break**

10:00   A Study of Multi-hop Mobile Communication Access Models Considering Elapsed Time from Coverage Area

Yukiko Nasu, Shigeru Shimamoto

10:20   Digital joint phase and sampling instant synchronisation for UMTS standard

Youssef Serrestou, Kosai RAOOF , Jo¸l LIENARD

10:40   Characterization of a Low Power, Short Range Wireless Transceiver

Usha Neupane, Samuel M. Richie, Arthur Weeks

11:00   Complex Spatial/Temporal CFAR

Ziba Ebrahimian, Hosein Alavi, Ali. M Doost Hoseini

11:20   The New Scheme for Data Rate Improvement in HF Communication without using Equalizer

Vahid Heidari, Mohammad H. Alavi

11:40   Fast Arithmetic of Elliptic Curve Cryptosystem in Mobile Communication

Zhang liang, Bian zhengzhong, Gao yingchun

April 7	8:00-10:00 AM	South Pacif
30	**Electromagnetic Compatibility and Interference**	

8:00   The Isolation Island and the Displacement of Decoupling Capacitors for Power Integrity Issues

Ding-Bing Lin, Chun-Te Wu, Guo-Chiang Hung

8:20   Shield Design about Circumference of Choke Structure Used
for Microwave Oven by Parallel FDTD

Kouta Matsumoto, Osamu Hashimoto

8:40   Graphical Analysis of Electromagnetic Coupling on B-737 and B-757 Aircraft for VOR and LOC IPL Data

Madiha Jafri, Linda Vahala, Jay Ely

9:00   Response Bounds Analysis for Transmission Lines Characterized by Uncertain Parameters

Sami Barmada, Antonino Musolino, Marco Raugi

9:20 Computational Electromagnetics Applied to Analyzing the Efficient Utilization of the RF Transmission Hyperspace

Andrew L. Drozd, Irina P. Kasperovich, Andrew C. Blackburn, Clifford E. Carroll, Jr., Chilukuri K. Mohan

9:40 Broadband Over Power Lines (BPL) Interference Analysis

Joel T. Fox

DEADLINE FOR THE SUBMISSION OF ARTICLES

Issue	Copy Deadline
March	February 1
July	June 1
November	October 1

For the ***ACES NEWSLETTER***, send copy to Bruce Archambeault in the following formats:

1. A PDF copy.
2. A MS Word (ver. 97 or higher) copy. If any software other than WORD has been used, contact the Managing Editor, Richard W. Adler **before** submitting a diskette, CD-R or electronic file.

Last Word

"The most exciting phrase to hear in science, the one that heralds the most discoveries, is not 'Eureka!' (I found it!) but 'That's funny...' "
Isaac Asimov